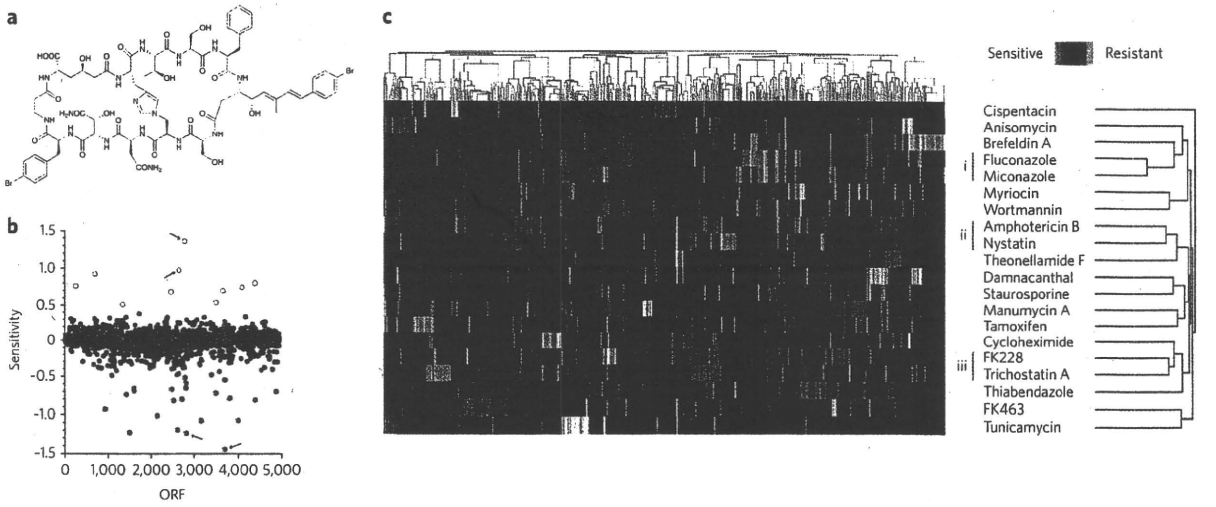

Figure 1 | Generation of chemical-genomic profiles. (**a**) Chemical structure of TNM-F. (**b**) Chemical-genomic profile of TNM-F. Ten ORFs conferring resistance (yellow) and 22 conferring hypersensitivity (blue) were identified (see **Supplementary Table 2** for detail). The *y* axis indicates the $\log_2$ of normalized AUC values, which were obtained from the growth curve of the corresponding transformant in the presence of various concentrations of TNM-F. Arrows indicate representative interactions: *SPCC23B6.04c* and *SPBC23G7.06c* are the top two resistance-conferring ORFs, whereas *SPAC26A3.09* (also known as *rga2*) and *SPAC17G8.14c* (also known as *pck1*) are the top two ORFs conferring hypersensitivity (see **Supplementary Fig. 2**). (**c**) Two-dimensional hierarchical clustering analysis of the 20 compound profiles. Compounds showing similar chemical-genomic profiles were clustered on the vertical axis; 575 ORFs are plotted on the horizontal axis on the basis the degree of hypersensitivity (blue) and resistance (yellow). Compounds possessing same target molecules are labeled with Roman numerals.

to overexpression of the gene product (**Supplementary Fig. 2**). Only a small subset, consisting of 169 strains that showed severe growth retardation upon overexpression, was excluded from our analysis (**Supplementary Data Set 1**). The overexpression strains were exposed individually to TNM-F and a compendium of ten reference compounds with known targets at various concentrations (**Supplementary Fig. 2** and **Supplementary Table 1**). Cell viability in liquid culture was measured using a colorimetric assay (XTT kit) and ranked quantitatively (**Supplementary Data Set 2**). Strains showing a significantly altered sensitivity compared to the control strain were selected and tested two more times. ORFs corresponding to the strains that were positive in all three rounds of screens were subjected to functional analysis (**Fig. 1b**, **Supplementary Data Set 3**).

We analyzed the chemical-genomic profiles by two-dimensional hierarchical clustering analysis[16] and compared the results with those obtained with TNM-F. The dendrogram suggested that these 11 compounds each function via distinct mechanisms (data not shown). To increase the profiles of target-known compounds, we selected approximately 600 strains that showed significant interactions with at least one of the 11 compounds and generated chemical-genetic profiles of nine other compounds using the selected strains (**Supplementary Table 1** and **Supplementary Data Set 4**). Thus, a total of 20 profiles were obtained, which we analyzed by two-dimensional hierarchical clustering analysis (**Fig. 1c**, **Supplementary Fig. 3** and **Supplementary Data Set 5**). We found a weak correlation with polyene antifungals amphotericin B (AMB) and nystatin (correlation coefficient = 0.18), implying that the mode of action of TNM-F is partially shared with these sterol binders.

In addition to pattern-matching analysis, information about the function of genes that alter sensitivity to the query compound (in other words, the hit genes) should be useful in predicting the target or its pathway. In the case of TNM-F, the gene conferring the strongest resistance was *SPCC23B6.04c*, which is predicted to encode a Sec14 homolog (**Supplementary Table 2**). The most sensitive strain overexpressed *SPAC26A3.09*, which encodes a homolog of Rho-type GTPase activating protein Rga2. The second most sensitive overexpressed *pck1*, which encodes a protein kinase C homolog that regulates 1,3-β-D-glucan synthesis[17].

We next determined GO terms with statistically significant enrichment ($P < 0.02$) in the hit genes for the initially tested 11 compounds and ranked them on the basis their extent of enrichment (**Supplementary Data Set 6**). This analysis showed that the hit genes for TNM-F were most enriched for GO terms related to cell polarity and signal transduction. However, none of these hit gene products appeared to be the primary target of TNM, because no physical interaction with immobilized TNM was detected (**Supplementary Fig. 1**). Furthermore, we carried out two-dimensional hierarchical clustering analysis of the enriched GO terms to compare with target-known compounds and found a modest linkage (correlation coefficient = 0.35) between TNM-F and FK463, a frontline clinical antifungal drug that inhibits the synthesis of 1,3-β-D-glucan[18] (**Supplementary Fig. 4**).

Counteraction of TNM-F with FK463

Of 32 TNM-F hit genes, 12 genes were in common with FK463, suggesting that modes of action of TNM-F and FK463 are functionally related (**Fig. 2a**). In contrast, TNM-F shared only two hit genes with nystatin. To see whether TNM-F also affects 1,3-β-D-glucan synthesis, we compared morphology of the cells after drug exposure. FK463 induced cell lysis at the growing ends in fungi by disrupting cell wall integrity (**Fig. 2b**), whereas TNM-F cells did not show any signs of cell lysis (**Fig. 2c,d**). Unexpectedly, however, calcofluor white (Cfw) staining showed strong signals at the growing ends and/or the medial region of the cells treated with TNM-F (**Fig. 2c,d**). Because TNM-F failed to increase the fluorescence in the *bgs1* mutant[19], in which the activity of the encoded 1,3-β-D-glucan synthase is greatly reduced (**Fig. 2e,f**), we suspected that the strong Cfw staining was due to increased 1,3-β-D-glucan synthesis. Similar images were also obtained using another fluorescent dye, aniline blue, which binds specifically to 1,3-β-D-glucans (**Supplementary Fig. 5**)[20]. AMB and nystatin did not increase the Cfw signal (**Fig. 2g**). Notably, the addition of TNM-F following FK463 treatment rescued the cells from FK463-induced cell lysis (**Fig. 2h**). Thus, TNM-F appears to

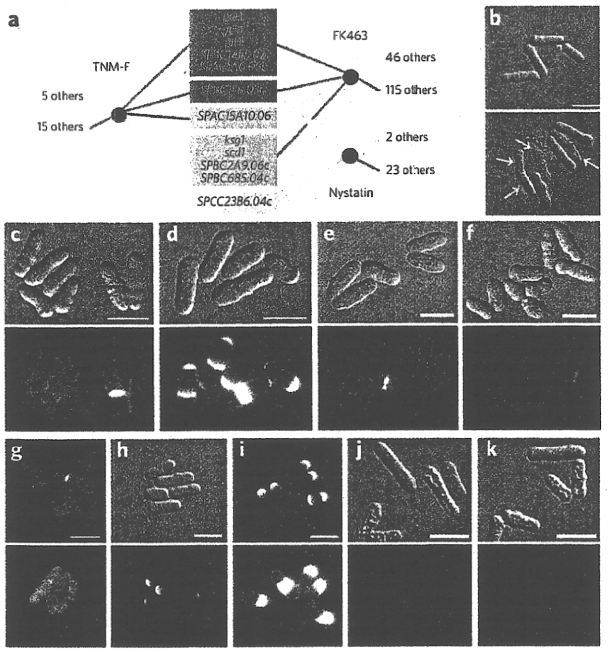

Figure 2 | Cell wall abnormality predicted by GO term analysis. (**a**) Chemical genetic interactions between TNM-F and FK463 or nystatin. Genes whose overexpression conferred resistance are shown in yellow, whereas those whose overexpression conferred hypersensitivity are shown in blue. Green boxes represent genes having opposite effects on TNM-F and FK463. (**b**) Cell lysis caused by FK463. Wild-type cells were treated with (lower) or without (upper) FK463 (20 μg ml^{-1}) for 2.5 h in the presence of 1.2 M sorbitol. FK463-treated cells showed the lysis phenotype (arrows). (**c**,**d**) Abnormal cell wall morphology induced by TNM-F. Yeast cells (HM123) were exposed to DMSO (**c**, 0.5% (v/v), solvent for TNM-F) or TNM-F (**d**, 5 μg ml^{-1}) for 2 h. (**e**,**f**) Bgs1 is required for aberrant Cfw staining by TNM-F. The strong Cfw signals were not observed in *bgs1* temperature-sensitive mutant cells incubated with DMSO (**e**, 0.5% (v/v)) or TNM-F (**f**, 5 μg ml^{-1}) at 27 °C for 2 h. (**g**) Effect of polyene antifungals on cell wall synthesis. Wild-type cells were treated with AMB (0.25 μg ml^{-1}, upper) or nystatin (1.6 μg ml^{-1}, lower) for 3 h. (**h**) Counteraction of FK463-induced cell lysis by TNM-F. (**i**–**k**) Involvement of Rho1 in the TNM-F–induced cell wall abnormality. Cells transformed with empty vector (**i**, upper), pREP41-Rho1 (**i**, lower) or pREP81-Rho1T20N (**j**,**k**) were grown at 30 °C for 15 h in MM liquid medium and then challenged with TNM-F (**i**,**k**) or DMSO (**j**) for an additional 2 h. Scale bars, 10 μm. In **c**–**k**, compound-treated cells were fixed and stained with Cfw. In **c**–**f**, **h**, **j** and **k**, differential interference contrast (DIC; upper) and Cfw (lower) images are shown.

counteract FK463 action by enhancing 1,3-β-D-glucan synthesis. Indeed, five genes identified as the hit genes of TNM-F and FK463 oppositely altered sensitivity to these compounds (**Fig. 2a**).

Rho1 mediates TNM-F–induced morphological abnormalities

1,3-β-D-Glucan is synthesized by transmembrane catalytic subunits in the presence of a regulatory subunit, a prenylated Rho1 (ref. 21). Rho1 is a small GTPase that plays a pivotal role in the signaling pathway involved in the regulation of cell polarity and in 1,3-β-D-glucan synthesis in fission yeast[21–23]. To test whether the TNM-induced 1,3-β-D-glucan synthesis is mediated by the activated Rho1 protein, we expressed a wild-type Rho1 in some cells and a dominant-negative Rho1 (Rho1T20N)[23] in others, using an inducible promoter. The overexpression of wild-type Rho1 greatly enhanced the Cfw staining induced by TNM-F (**Fig. 2i**). On the other hand, overexpression of Rho1T20N clearly inhibited the TNM-induced 1,3-β-D-glucan synthesis (**Fig. 2j,k**). Thus, the action of TNM-F appears to require Rho1. Rho1's effects are mediated by its interaction with at least three targets: 1,3-β-D-glucan synthase[21] and the protein kinases Pck1 and Pck2 (ref. 17,24), all of which are involved in 1,3-β-D-glucan synthesis. Deletion of neither *pck1* nor *pck2* abolished the increased Cfw staining induced by TNM-F (**Supplementary Fig. 6**). These results suggest that the major pathway to 1,3-β-D-glucan synthesis upon TNM-F treatment is the direct activation of Bgs1 by Rho1. However, Rho1T20N did not suppress the binding and cytotoxicity of TNM (**Supplementary Figs. 7** and **8**), suggesting that aberrant 1,3-β-D-glucan synthesis is not the primary reason for the TNM's cytotoxicity.

TNMs bind to 3β-hydroxysterols

To determine the subcellular localization of the TNM-binding molecule, we synthesized a fluorescently labeled TNM derivative (**3**, **4**, TNM-BF) by conjugating a 4,4-difluoro-5,7-dimethyl-4-bora-3a, 4a-diaza-*s*-indacene-3-propionic acid moiety (BODIPY-FL) to the β-D-galactose moiety of TNM-A (**Supplementary Fig. 9**). TNM-BF was as active as TNM-F in inhibiting cell growth of wild-type *S. pombe* (**Supplementary Fig. 10**). Fluorescence microscopy clearly showed that TNM-BF is distributed at cell tips and in the septation region of cells undergoing cytokinesis (**Fig. 3a**). According to our Localizome dataset (available here: http://www.riken.jp/SPD/index.html), which assigned each of the 4,429 proteins to one of 17 possible subcellular localizations[13], approximately 80 proteins showed similar localization to TNM-BF (**Supplementary Data Set 7**). GO analysis revealed that transmembrane transporters were significantly enriched among these proteins (**Supplementary Table 3**). Transporters and lipid molecules have a close functional relationship (for example, Pma1 (**Fig. 3b**) is a marker for the lipid raft[25], a characteristic membrane microdomain rich in ergosterol and sphingolipids[26]). The proper localization of Pma1 depends on ergosterol biosynthesis[27]. On the basis of these observations, we theorized that the target of TNM could be a lipid molecule distributed in a polarized manner, rather than a protein. A binding assay using plasma membrane lipid components revealed that TNM-BF selectively recognizes ergosterol but not other lipids tested (**Fig. 3c**). In addition to ergosterol, TNM-BF bound to cholesterol, cholestanol and 5α-cholest-7-en-3β-ol (**Fig. 3d,e**). In contrast, a ketone group, an α-hydroxyl group or an esterification of the hydroxyl group at C3 position abolished the binding, indicating that TNM recognizes 3β-hydroxysterols (**Fig. 3e**).

Filipin, a fluorescent compound that forms a specific complex with 3β-hydroxysterols in the cell membrane[28], stained the cell periphery and medial region of cells undergoing cytokinesis[29] in a pattern very similar to that of TNM-BF, suggesting that the target of TNM-F in wild-type *S. pombe* is ergosterol, the major sterol in fungi. Double staining showed a clear overlap of the signals for the two compounds, but the region stained with TNM-BF was slightly more confined (**Fig. 3f**).

In vivo ergosterol distribution is regulated in a cell cycle–dependent manner in fission yeast[29], probably as a result of some function of actin[25,30]. Indeed, we also observed that latrunculin A treatment disrupted the polarity of filipin staining (**Supplementary Fig. 11**). Notably, latrunculin A reduced the fluorescent signal of TNM-BF to an almost undetectable level. Similarly, in a strain possessing an *act1* (also known as *cps8*) temperature-sensitive allele[30,31] both filipin and TNM-BF stained the cell tips and around the septum, as observed in wild-type cells at the permissive temperature, but their polarized localization was lost after temperature shift (**Supplementary Fig. 11**). It should be noted that the decrease in TNM-BF fluorescence was again observed in the *act1* mutant cells at 30 °C. It seems possible that proper organization of the sterol-rich membrane domain is required for TNM binding of the cell membrane. Indeed, overexpression of hit genes *scd1* and *rga2*, both

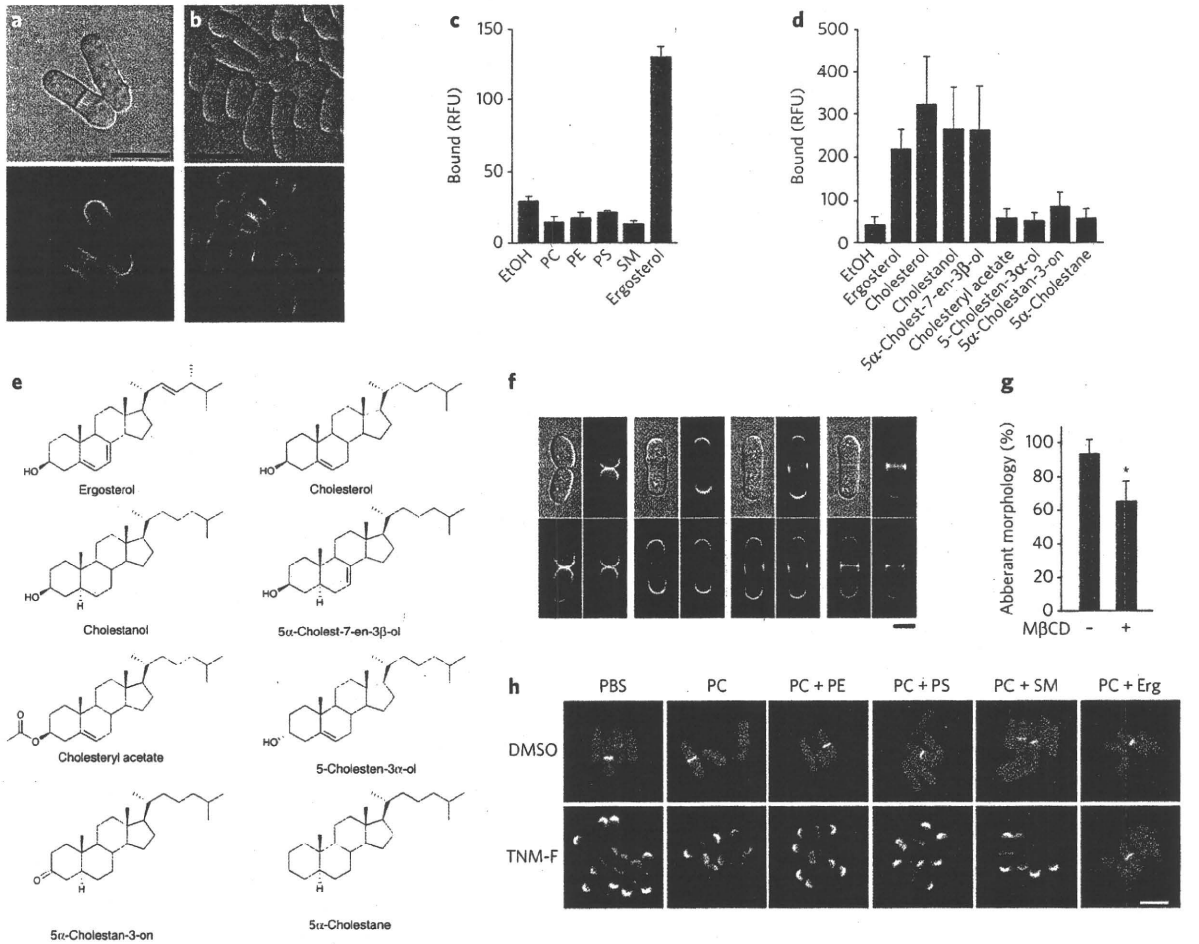

Figure 3 | Identification of 3β-hydroxysterols as the target of TNM-F. (**a**) The fluorescent image of cells stained by TNM-BF. (**b**) An example of protein localization similar to TNM-BF localization. The fluorescent image of the YFP-fused Pma1 is shown. (**c**) Binding of TNM-BF to ergosterol *in vitro*. (**d**) Binding of TNM-BF to various sterols *in vitro*. (**e**) Structure-affinity relationships of sterols. Functionalities colored in blue are not necessary for recognition by TNM-BF, whereas the red-colored structures hamper binding to TNM-BF. (**f**) Co-localization of TNM-BF with filipin. TNM-BF (upper right panels and red in merged images) and filipin (lower left panels and green in merged images) signals were observed in the similar region. Images of cells at different cell cycle stages are shown. (**g**) Effects of ergosterol extraction on the TNM-F–induced cell wall abnormality. Cells were preincubated in the presence (+) or absence (−) of methyl-β-cyclodextrin (MβCD) and then treated with TNM-F. After Cfw staining, cells with abnormally strong signals were counted. Asterisk indicates statistically significant difference ($P < 0.02$). See **Supplementary Figure 13** for details. (**h**) Effects of ergosterol-containing vesicles on TNM-F–induced cell wall abnormalities. Cells were treated with TNM-F (5 μg ml^{-1}) that had been preincubated with POPC vesicles or POPC-based vesicles containing PE (PC + PE), PS (PC + PS), SM (PC + SM) or ergosterol (PC + Erg) for 30 min. After 3 h incubation with TNM-F, cells were fixed and stained with Cfw. Scale bars are 10 μm except that in **f**, which is 5 μm. Data represent means of three (**c**,**d**) or four (**g**, $n > 110$ for each experiment) independent experiments. In **c**,**d** and **g**, error bars indicate s.d. RFU: Relative fluorescence units.

of which are involved in regulation of the actin cytoskeleton[32–34], caused a drastic decrease and increase, respectively, in TNM-BF staining (**Supplementary Fig. 12**).

Sterol binding is required for action of TNM-F

We next determined whether 3β-hydroxysterols are also required for TNM-induced 1,3-β-D-glucan synthesis. First, pretreatment of cells with methyl-β-cyclodextrin, which could extract a substantial amount of ergosterol (**Supplementary Fig. 13**), significantly reduced the number of cells showing an enhanced Cfw signal (**Fig. 3g**). Second, preincubation of TNM-F with 1-palmitoyl-2-oleoyl-*sn*-glycero-3-phosphocholine (POPC)-based multilamellar vesicles did not affect TNM-enhanced Cfw staining, but preincubation with vesicles containing ergosterol abolished it (**Fig. 3h**). These results suggest that pre-absorption of TNM-F with the ergosterol-rich membrane alleviates the action of TNM-F. Furthermore, latrunculin A treatment, which inhibits TNM-BF binding of cells, also hampered the TNM-F–induced abnormal Cfw staining (**Supplementary Fig. 14**). Thus, we conclude that a structured membrane domain rich in ergosterol and related sterols is required for the binding of TNM-F to exert its effects on the cell wall.

Effects of *erg* mutations on TNM-F sensitivity

Genetic mutations in the ergosterol biosynthetic pathway (**Fig. 4a**) have been shown to modulate sensitivity to polyene antibiotics in yeast[27,35]. In *S. pombe erg* mutants, ergosterol production is not detectable; however, filipin staining is not abolished, implying that sterols with filipin-binding activity other than ergosterol can still be produced and that they compensate for the roles of ergosterol[27]. Lack of Erg2, the putative enzyme that converts fecosterol to episterol, or simultaneous deletion of two *erg3*$^+$ homologs, *erg31* and *erg32*, both of which encode putative enzymes catalyzing the

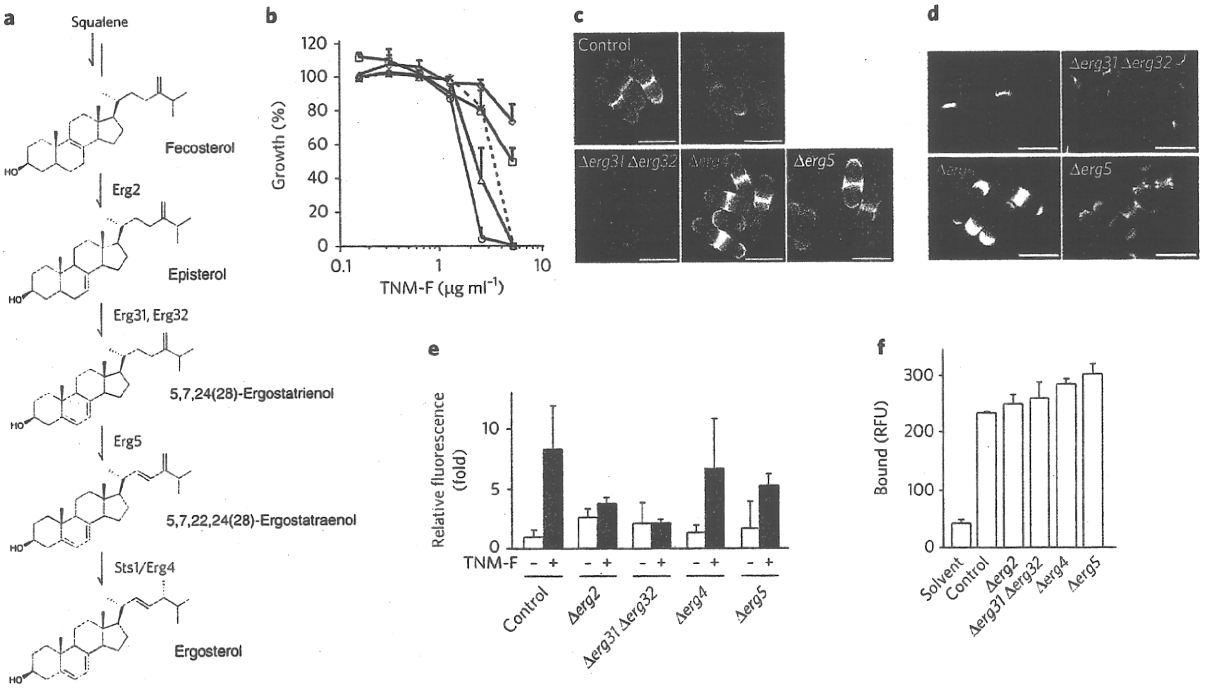

Figure 4 | Genetic interactions with ergosterol biosynthetic genes. (**a**) Ergosterol biosynthesis pathway. (**b**) TNM-F sensitivity of *erg* mutants, Δ*erg2* (solid blue); Δ*erg31* Δ*erg32* (solid red); Δ*sts1/erg4* (solid green); Δ*erg5* (dashed black); and the control strain HM123 (solid black). Data represent means of three independent experiments. Error bars, s.d. (**c**) Localization of TNM-BF-binding molecules in *erg* mutant cells. Cells were treated with TNM-BF (2.5 μg ml^{-1}) at 30 °C for 1 h, and the fluorescence was observed. (**d**,**e**) Effects of mutations in the ergosterol biosynthetic pathway on the TNM-F-induced cell wall abnormality. Various *erg* mutants were treated with TNM-F, and the extent of abnormal cell wall synthesis was determined using Cfw staining. Quantitation of the fluorescence intensity is shown in **e**. Relative intensities to the control cells treated with DMSO were determined. Error bars represent s.d. of three independent experiments ($n \geq 9$ for each experiment). (**f**) Binding of TNM-BF to the sterol fractions prepared from various *erg* mutant cells. Data represent means of three independent experiments. Error bars, s.d.; scale bars, 10 μm.

reaction from episterol to 5,7,24(28)-ergostatrienol, caused ergosterol deficiency and apparent tolerance to polyene antibiotics[27]. These *erg* mutants were also highly tolerant to TNM-F (**Fig. 4b**). On the other hand, deletion of *erg5* conferred modest resistance to TNM-F, and only marginal resistance was observed in Δ*sts1/erg4* cells (**Fig. 4b**). However, deletion of *dsd1* (ref. 36) or *SPBC887.15c*, both encoding enzymes involved in sphingolipid metabolism, did not affect the sensitivity to TNM-F. But Δ*SPBC887.15c* cells were specifically resistant to syringomycin E (**Supplementary Fig. 15**). The ability of TNM-BF to bind to cells correlated well with their sensitivity to TNM-F (**Fig. 4c**). The extent of the abnormality in cell wall architecture in the TNM-F-treated *erg* mutant cells correlated with their TNM sensitivity as well as binding capacity (**Fig. 4d**,**e** and **Supplementary Fig. 16**). However, *in vitro* binding experiments showed similar TNM-BF binding of the sterol fractions isolated from all *erg* deletion strains (**Fig. 4f**), indicating that TNMs bind to other cellular sterols *in vitro*. It is likely that changes in the state of the plasma membrane in the *erg* mutants render TNM-F less readily accessible to membrane sterols. Indeed, the ability to bind to filipin was also reduced in the Δ*erg2* and Δ*erg31* Δ*erg32* cells (**Supplementary Fig. 17**)[27], indicating the modulated accessibility of 3β-hydroxysterols in the membrane of these mutants.

Effects of TNM-F on plasma membrane integrity

To further examine whether TNM binding of the sterol-rich membrane affects yeast plasma membrane integrity, we added the fluorescent dye calcein to the *S. pombe* cells that had been treated with TNM-F for 9 h. Passive entry of calcein over the plasma membrane was observed upon treatment with TNM-F, indicating that cells cannot retain the membrane integrity in the presence of TNM-F (**Fig. 5a**). Calcein diffusion following TNM-F exposure increased in a dose-dependent manner (**Fig. 5b**). Time-course experiments showed that the calcein diffusion into the TNM-F–treated cells gradually increased over time (**Fig. 5c**). In contrast, the elevated 1,3-β-D-glucan synthesis occurred very rapidly, and 1 h treatment was sufficient for the induction of 1,3-β-D-glucan synthesis in most cells at the concentration of 5 μg ml^{-1}(**Supplementary Fig. 18**). Consistent with the TNM susceptibility (**Fig. 4b**), binding (**Fig. 4c**) and Cfw staining (**Fig. 4d**,**e**) data, no significant diffusion of calcein was observed in Δ*erg2* and Δ*erg31* Δ*erg32* cells (**Fig. 5d**), suggesting a direct link between TNM-F binding and the observed effects, including loss of membrane integrity.

Comparison with polyene antifungals

Lastly, we asked whether the mode of action of TNM is identical to that of the conventionally used polyene antibiotics. The most typical morphological change of yeast cells after treatment with polyene antibiotics is the enlargement of vacuoles (**Fig. 5e**,**f**)[37]. This phenomenon was not observed in the TNM-F–treated cells; instead, the vacuoles became highly fragmented (**Fig. 5g**). In contrast to the vacuoles of AMB-treated cells, which leaked vacuolar-specific dye (CDCFDA) to the cytosol, the fragmented vacuoles in the TNM-F-treated cells retained the dye, suggesting that the vacuolar membrane damage is marginal. Rho1 may also be involved in vacuole fragmentation induced by TNM because overexpression of wild-type Rho1 caused similar vacuole fragmentation, and Rho1T20N alleviated the TNM-induced vacuole abnormality (**Supplementary Fig. 19**).

The other characteristic aspect of polyene antifungals is their acute fungicidal effect: most cells died shortly after AMB treatment, and no

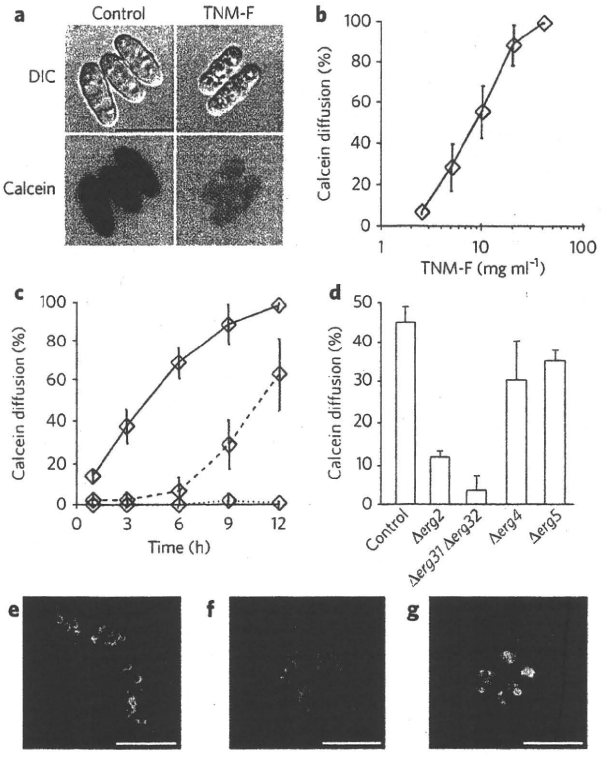

Figure 5 | Disruption of plasma membrane integrity by TNM-F. (**a**) Dye exclusion assay for testing plasma membrane integrity using calcein, a membrane-impermeable fluorescent dye. Passive entry of calcein into *S. pombe* cells was induced by TNM-F (20 μg ml^{-1} for 9 h). In the absence of TNM-F, calcein diffusion was rarely observed. (**b**,**c**) Kinetics of calcein diffusion induced by TNM-F. The dye diffusion was observed in a manner dependent on concentration (**b**) and time (**c**). Incubation time in **b** was 9 h. Cells were incubated without (dotted line) or with 5 μg ml^{-1} (dashed line) or 20 μg ml^{-1} (solid line) of TNM-F in **c**. (**d**) Effects of *erg* mutations on TNM-F-induced membrane damage. Calcein diffusion was attenuated in *Δerg2* or *Δerg31 Δerg32* cells. Data in **b**-**d** represent means of three independent experiments ($n > 10$ for each experiment). Error bars, s.d. (**e**-**g**) Changes in vacuole morphology. Wild-type cells stained with CDCFDA (green) and FM4-64 (red) were exposed to DMSO (**e**, 1% (v/v)), AMB (**f**, 5 μg ml^{-1}) or TNM-F (**g**, 10 μg ml^{-1}) for 1 h. Scale bars, 10 μm.

time-dependent cell death was observed (**Supplementary Fig. 20**). In contrast, TNM-F showed time-dependent toxicity, with similar kinetics to that of the calcein diffusion (**Fig. 5c** and **Supplementary Fig. 20**). Taken together with the inability of AMB or nystatin to increase 1,3-β-D-glucan synthesis (**Fig. 2g**), these data caused us to conclude that TNM-F is a previously undescribed sterol-binding molecule and that its mode of action is distinct from that of polyene antibiotics.

DISCUSSION

Marine invertebrates, including marine sponges, are an important source for numerous biologically active compounds, which are often synthesized by symbiotic microorganisms[38]. Bicyclic peptides, such as theonellamides (TNMs), are a family of marine natural products with potent antifungal activity. Despite extensive efforts to isolate the TNM-binding proteins, the modes of action of these compounds have been heretofore unknown. Recently, a mutation in *MVD1*, also known as *ERG19*, encoding an essential enzyme involved in an early step in the ergosterol biosynthesis pathway was shown to be specifically resistant to theopalauamide in *Saccharomyces cerevisiae*[39], suggesting a link between the drug target and the ergosterol biosynthetic pathway. In this study, by taking advantage of a chemical-genomic screen for the genes that alter TNM sensitivity when overexpressed, we demonstrated that TNM specifically binds to a class of lipid molecules (3β-hydroxysterols), rather than a protein, in the fission yeast.

The idea that ergosterol, the major sterol molecule in fungi, is the target of TNM in fission yeast is supported not only by the compound's physical interaction with 3β-hydroxysterols, including ergosterol, but also by several lines of genetic and biochemical evidence. Mutants defective in ergosterol biosynthesis (*Δerg2* and *Δerg31 Δerg32*) showed drastically increased tolerance to TNM and a decreased ability of the cells to bind TNM. Drug sensitivity was well correlated with *in vivo* TNM binding of the membrane. Indeed, TNM-BF binding of the cells overexpressing *SPCC23B6.04c*, the gene conferring the highest resistance, was very low (**Supplementary Fig. 12**). In contrast, *in vitro* binding of TNM-BF to the extracted sterol fraction was independent of susceptibilities of the *erg* mutants, suggesting that TNM-BF binds to sterol metabolites other than ergosterol *in vitro*, and that the accessibility of these 3β-hydroxysterols and the membrane architectures determine the efficient binding of TNM to the plasma membrane *in vivo*. The observation that defects in actin impaired polarized distribution of sterols[30] and greatly reduced *in vivo* TNM binding also supports the notion that proper organization of the membrane domain is prerequisite for *in vivo* TNM binding of the membrane sterols.

TNM binding 3β-hydroxysterols in the membrane initially induced overproduction of the cell wall component 1,3-β-D-glucan. *S. pombe* Rho1 GTPase regulates 1,3-β-D-glucan synthase and is required for the maintenance of cell wall integrity and polarization of the actin cytoskeleton[21,23]. Our mutational analyses demonstrated that TNM triggers the onset of signaling mediated by Rho1 GTPase to directly activate 1,3-β-D-glucan synthase. TNM treatment led to rapid accumulation of 1,3-β-D-glucan at the cell tips and the site of cytokinesis (**Fig. 5c** and **Supplementary Fig. 18**), which are essentially the same regions stained by filipin and TNM-BF, implying that 1,3-β-D-glucan synthase is also localized within or adjacent to the lipid microdomains. Rho1 may also be involved in vacuole fragmentation induced by TNM (**Supplementary Fig. 19**).

A later biological consequence of TNM binding the sterol-rich membrane was the induction of membrane damage. Indeed, the dye exclusion assay showed that the integrity of the plasma membrane in *S. pombe* was damaged by TNM in an incubation time–dependent manner, thereby reducing cell viability. Although TNM induced aberrant 1,3-β-D-glucan synthesis by Rho1 activation, it may be independent of the TNM-induced cytotoxic membrane damage, as the overexpression of Rho1T20N did not suppress the TNM-BF binding the cell membrane (**Supplementary Fig. 7**) and cytotoxicity of TNM-F (**Supplementary Fig. 8**). The polyene antifungals also form pores in the lipid bilayer by interacting with ergosterol, thereby causing leakage of cytosolic constituents such as ions[40]. However, the mode of action of TNM-F is apparently distinct from that of polyene antifungals because the phenotypic changes induced by these two families of antifungals are different. Not all the *erg* mutants prevented TNM binding and damage to membrane. What has been established is the correlation between the TNM's effects on cells and its efficient binding to plasma membrane *in vivo* (**Fig. 4** and **Supplementary Fig. 12**). It is most likely that the binding of TNM-F requires not only sufficient content of ergosterol and other 3β-hydroxysterols but also the proper membrane architecture. In that sense, TNM resembles lysenin, a sphingomyelin-specific toxin isolated from the coelomic fluid of the earthworm *Eisenia foetida*, which has been shown to bind clusters of sphingomyelin in the membrane[41]. Thus, TNM represents a previously unknown class of sterol-binding molecules.

In summary, we have discovered that TNM represents a previously undescribed, mechanistically distinct class of sterol-binding molecules, a powerful tool for exploring the function and localization of sterols in cells. It remains to be determined how TNM binds to sterols in plasma membrane *in situ* and activates Rho1-mediated 1,3-β-D-glucan synthesis, as well as other processes that lead subsequently to membrane damage and cytotoxicity. To develop practical antifungal drugs from such large and complex natural products, it will also be critical to perform structure-function relationship studies to identify the minimal chemical structure essential for TNM's biological activity.

METHODS

Chemical compounds. Thiabendazole and damnacanthal were purchased from Wako Pure Chemical Industries. Other compounds for chemical-genomic profiling were purchased from Sigma. FK463 and cispentacin were gifts from A. Fujie, Astellas Pharma. Trichostatin A and FK228 were from the laboratory collection. TNM-F was isolated from a marine sponge *Theonella* sp. as described previously[8]. The fluorescent derivative of TNM was prepared as described in the **Supplementary Methods**. 1,2-Dimyristoyl-*sn*-glycero-3-phosphocholine (DMPC), 1,2-dimyristoyl-*sn*-glycero-3-phosphoethanolamine (DMPE), and methyl-β-cyclodextrin were purchased from Wako Pure Chemical Industries, Ltd. 1-Palmitoyl-2-oleoyl-*sn*-glycero-3-phosphocholine (POPC), 1,2-dimyristoyl-*sn*-glycero-3-phospho-L-serine (DMPS), chicken egg yolk sphingomyelin (SM), cholesterol, cholestanol, 5α-cholest-7-en-3β-ol, cholesteryl acetate, 5α-cholestan-3-on, 5α-cholestane, calcofluor white, filipin, latrunculin A and syringomycin E were from Sigma. Ergosterol was from Nacalai Tesque, 5-cholesten-3α-ol was from Steraloids Inc., calcein was from Dojindo Laboratories and CDCFDA and FM4-64 were from Molecular Probes Inc.

Yeast strains. *S. pombe* strains used in this study are JY1 (*h⁻*), HM123 (*h⁻ leu1-32*), *erg* mutants (*h⁻ ura4-C190T leu1-32 erg2::ura4⁺*, *h⁻ ura4-C190T leu1-32 erg31::ura4-FOA^R erg32::ura4⁺*, *h⁻ ura4-C190T leu1-32 erg4::ura4⁺*, and *h⁻ ura4-C190T leu1-32 erg5::ura4⁺*)[27], and KP165 (*h⁻ leu1-32 bgs1-i2*)[19]. Fission yeast overexpression strains derived from AM2 (*h^90 leu1-32*) were generated using the multipurpose plasmid pDUAL-FFH1c[12] as described previously[13].

Preparation of chemical-genomic profiles. Overexpression strains were initially grown on SD solid medium at 30 °C for 2–3 d. To allow expression, each strain was subsequently grown in 200 μL of minimal medium in 96-well plates at 30 °C for 48 h with vigorous shaking. Expression-induced cell cultures were diluted at 1:2,000 and exposed to compounds at 30 °C for 24 h in 100 μL minimal medium in 96-well plates. Cell growth was assessed by the degree of respiration (an XTT assay) using a Cell Proliferation Kit II (Roche, Switzerland). Secondary screens were carried out on strains showing significantly altered sensitivity in the primary screen. The sensitivity of the strain was quantified by calculating the area under the curve (AUC) of growth versus dose (*x* axis: compound concentration; *y* axis: cell growth (%)), normalized against the median AUC value of all strains in each experiment. Strains with significantly altered normalized AUC values in the secondary screen were tested again; in this trial, the obtained AUC value was normalized against the AUC value from the control strain (**Supplementary Data Sets 2** and **3**).

Preparation of compound profiles using a minimal strain set. See **Supplementary Methods** for experimental procedures.

Clustering analysis. See **Supplementary Methods** and **Supplementary Dataset 8** for experimental procedures.

Functional analysis of the chemical-genomic profiles with GO terms. See **Supplementary Methods** for experimental procedures.

Lipid-binding assay. The ability of TNM-BF to bind to various lipid species was evaluated in a microtiter plate. The wells of microtiter plates (Immulon 1B, Thermo Fisher Scientific, Inc.) were coated with lipid solution (50 μM of DMPC, DMPE, DMPS, sterols (10 μM each), SM (10 μg ml⁻¹), or 40 μl of yeast sterol fractions (10 μg ml⁻¹)) in ethanol by evaporating at 30 °C for 2 h. After blocking the wells with Tris-buffered saline (10 mM Tris-HCl, pH 7.4, 150 mM NaCl) containing 1% (v/v) skim milk (BD) (buffer A) for 1 h at 30 °C, the wells were incubated with TNM-BF (1.0 μg ml⁻¹) in buffer A for 1 h at 30 °C. After washing the wells twice with buffer A, we dissolved the bound TNM-BF in 50 μl of DMSO, 40 μl of which was transferred to another 96-well plate (FIA black module plate, Greiner Bio-One) to measure the bound fluorescence (excitation 490 nm, emission 528 nm) using a SpectraMax M2e microplate reader (Molecular Devices). Yeast sterol fractions were prepared as described previously[27].

Drug sensitivity test. See **Supplementary Methods** for experimental procedures.

Microscopy. Cells were treated with compounds at 30 °C unless stated otherwise in the figure legend. Multilamellar vesicle competition was carried out using POPC-based vesicles. In detail, TNM-F (10 μg ml⁻¹) was preincubated with POPC vesicles or POPC-based vesicles (100 μM of total lipid concentration) containing 20 mol % of DMPE, DMPS, SM or ergosterol for 30 min. Cells were incubated with this mixture for 3 h (final concentration of TNM-F is 5 μg ml⁻¹ and that of total lipid is 50 μM), then fixed and stained with Cfw. For Cfw staining, fixed cells were suspended in a buffer (100 mM PIPES, pH 6.9, 1 mM EGTA, 1 mM $MgSO_4$) containing Cfw. Cell lysis by FK463 was observed as described in **Supplementary Methods**. Visualization of sterols using filipin was carried out as described[29]. For the co-localization study, cells were exposed to TNM-BF (2.5 μg ml⁻¹) for 30 min, followed by filipin staining. Vacuole morphology was visualized with FM4-64 and CDCFDA as described[43]. Dye exclusion assay was carried in the presence of calcein at a concentration of 50 μg ml⁻¹. To collect images, we used either a DeltaVision system (Applied Precision) with an Olympus IX70 fluorescence microscope equipped with an UPlan Apo ×100 lens, or a MetaMorph system (Universal Imaging Corp.) with an Olympus IX81 fluorescence microscope equipped with an UPLSAPO ×100 lens. Quantitation of the intensity of the Cfw fluorescence was carried out using MetaMorph software.

Received 6 February 2009; accepted 23 March 2010; published online 13 June 2010

References

1. Baltz, R.H. Daptomycin: mechanisms of action and resistance, and biosynthetic engineering. *Curr. Opin. Chem. Biol.* **13**, 144–151 (2009).
2. Denning, D.W. Echinocandin antifungal drugs. *Lancet* **362**, 1142–1151 (2003).
3. Rovira, P., Mascarell, L. & Truffa-Bachi, P. The impact of immunosuppressive drugs on the analysis of T-cell activation. *Curr. Med. Chem.* **7**, 673–692 (2000).
4. Dawson, S., Malkinson, J.P., Paumier, D. & Searcey, M. Bisintercalator natural products with potential therapeutic applications: isolation, structure determination, synthetic and biological studies. *Nat. Prod. Rep.* **24**, 109–126 (2007).
5. Kong, D. *et al.* Echinomycin, a small-molecule inhibitor of hypoxia-inducible factor-1 DNA-binding activity. *Cancer Res.* **65**, 9047–9055 (2005).
6. Vera, M.D. & Joullie, M.M. Natural products as probes of cell biology: 20 years of didemnin research. *Med. Res. Rev.* **22**, 102–145 (2002).
7. Matsunaga, S. & Fusetani, N. Nonribosomal peptides from marine sponges. *Curr. Org. Chem.* **7**, 945–966 (2003).
8. Matsunaga, S., Fusetani, N., Hashimoto, K. & Walchli, M. Theonellamide-F - a novel antifungal bicyclic peptide from a marine sponge *Theonella* sp. *J. Am. Chem. Soc.* **111**, 2582–2588 (1989).
9. Matsunaga, S. & Fusetani, N. Theonellamides A–E, cytotoxic bicyclic peptides, from a marine sponge *Theonella* sp. *J. Org. Chem.* **60**, 1177–1181 (1995).
10. Bewley, C.A. & Faulkner, D.J. Theonegramide, an antifungal glycopeptide from the Philippine lithistid sponge *Theonella swinhoei*. *J. Org. Chem.* **59**, 4849–4852 (1994).
11. Schmidt, E.W., Bewley, C.A. & Faulkner, D.J. Theopalauamide, a bicyclic glycopeptide from filamentous bacterial symbionts of the lithistid sponge *Theonella swinhoei* from Palau and Mozambique. *J. Org. Chem.* **63**, 1254–1258 (1998).
12. Wada, S., Matsunaga, S., Fusetani, N. & Watabe, S. Interaction of cytotoxic bicyclic peptides, theonellamides A and F, with glutamate dehydrogenase and 17beta-hydroxysteroid dehydrogenase IV. *Mar. Biotechnol. (NY)* **2**, 285–292 (2000).
13. Matsuyama, A. *et al.* ORFeome cloning and global analysis of protein localization in the fission yeast *Schizosaccharomyces pombe*. *Nat. Biotechnol.* **24**, 841–847 (2006).
14. Shirai, A. *et al.* Global analysis of gel mobility of proteins and its use in target identification. *J. Biol. Chem.* **283**, 10745–10752 (2008).
15. Kanoh, N., Honda, K., Simizu, S., Muroi, M. & Osada, H. Photo-cross-linked small-molecule affinity matrix for facilitating forward and reverse chemical genetics. *Angew. Chem. Int. Edn Engl.* **44**, 3559–3562 (2005).
16. Hughes, T.R. *et al.* Functional discovery via a compendium of expression profiles. *Cell* **102**, 109–126 (2000).
17. Arellano, M. *et al.* *Schizosaccharomyces pombe* protein kinase C homologues, pck1p and pck2p, are targets of rho1p and rho2p and differentially regulate cell integrity. *J. Cell Sci.* **112**, 3569–3578 (1999).
18. Tomishima, M. *et al.* FK463, a novel water-soluble echinocandin lipopeptide: synthesis and antifungal activity. *J. Antibiot. (Tokyo)* **52**, 674–676 (1999).
19. Deng, L. *et al.* Phosphatidylinositol-4-phosphate 5-kinase regulates fission yeast cell integrity through a phospholipase C-mediated protein kinase C-independent pathway. *J. Biol. Chem.* **280**, 27561–27568 (2005).
20. Kippert, F. & Lloyd, D. The aniline blue fluorochrome specifically stains the septum of both live and fixed *Schizosaccharomyces pombe* cells. *FEMS Microbiol. Lett.* **132**, 215–219 (1995).
21. Arellano, M., Duran, A. & Perez, P. Rho 1 GTPase activates the (1–3) beta-D-glucan synthase and is involved in *Schizosaccharomyces pombe* morphogenesis. *EMBO J.* **15**, 4584–4591 (1996).

22. Arellano, M., Duran, A. & Perez, P. Localisation of the *Schizosaccharomyces pombe* rho1p GTPase and its involvement in the organisation of the actin cytoskeleton. *J. Cell Sci.* **110**, 2547–2555 (1997).
23. Nakano, K., Arai, R. & Mabuchi, I. The small GTP-binding protein Rho1 is a multifunctional protein that regulates actin localization, cell polarity, and septum formation in the fission yeast *Schizosaccharomyces pombe*. *Genes Cells* **2**, 679–694 (1997).
24. Sayers, L.G. *et al.* Rho-dependence of *Schizosaccharomyces pombe* Pck2. *Genes Cells* **5**, 17–27 (2000).
25. Takeda, T., Kawate, T. & Chang, F. Organization of a sterol-rich membrane domain by cdc15p during cytokinesis in fission yeast. *Nat. Cell Biol.* **6**, 1142–1144 (2004).
26. Simons, K. & Ikonen, E. Functional rafts in cell membranes. *Nature* **387**, 569–572 (1997).
27. Iwaki, T. *et al.* Multiple functions of ergosterol in the fission yeast *Schizosaccharomyces pombe*. *Microbiology* **154**, 830–841 (2008).
28. Drabikowski, W., Lagwińska, E. & Sarzala, M.G. Filipin as a fluorescent probe for location of cholesterol in membranes of fragmented sarcoplasmic reticulum. *Biochim. Biophys. Acta* **291**, 61–70 (1973).
29. Wachtler, V., Rajagopalan, S. & Balasubramanian, M.K. Sterol-rich plasma membrane domains in the fission yeast *Schizosaccharomyces pombe*. *J. Cell Sci.* **116**, 867–874 (2003).
30. Codlin, S., Haines, R.L. & Mole, S.E. btn1 affects endocytosis, polarization of sterol-rich membrane domains and polarized growth in *Schizosaccharomyces pombe*. *Traffic* **9**, 936–950 (2008).
31. Ishiguro, J. & Kobayashi, W. An actin point-mutation neighboring the 'hydrophobic plug' causes defects in the maintenance of cell polarity and septum organization in the fission yeast *Schizosaccharomyces pombe*. *FEBS Lett.* **392**, 237–241 (1996).
32. Villar-Tajadura, M.A. *et al.* Rga2 is a Rho2 GAP that regulates morphogenesis and cell integrity in *S. pombe*. *Mol. Microbiol.* **70**, 867–881 (2008).
33. Chang, E.C. *et al.* Cooperative interaction of *S. pombe* proteins required for mating and morphogenesis. *Cell* **79**, 131–141 (1994).
34. Iwaki, N., Karatsu, K. & Miyamoto, M. Role of guanine nucleotide exchange factors for Rho family GTPases in the regulation of cell morphology and actin cytoskeleton in fission yeast. *Biochem. Biophys. Res. Commun.* **312**, 414–420 (2003).
35. Hampsey, M. A review of phenotypes in *Saccharomyces cerevisiae*. *Yeast* **13**, 1099–1133 (1997).
36. Garton, S., Michaelson, L.V., Beaudoin, F., Beale, M.H. & Napier, J.A. The dihydroceramide desaturase is not essential for cell viability in *Schizosaccharomyces pombe*. *FEBS Lett.* **538**, 192–196 (2003).
37. Takeo, K. *et al.* Rapid, extensive and reversible vacuolation of *Schizosaccharomyces pombe* induced by amphotericin B. *FEMS Microbiol. Lett.* **108**, 265–269 (1993).
38. Piel, J. Bacterial symbionts: prospects for the sustainable production of invertebrate-derived pharmaceuticals. *Curr. Med. Chem.* **13**, 39–50 (2006).
39. Ho, C.H. *et al.* A molecular barcoded yeast ORF library enables mode-of-action analysis of bioactive compounds. *Nat. Biotechnol.* **27**, 369–377 (2009).
40. Bolard, J. How do the polyene macrolide antibiotics affect the cellular membrane properties? *Biochim. Biophys. Acta* **864**, 257–304 (1986).
41. Shogomori, H. & Kobayashi, T. Lysenin: a sphingomyelin specific pore-forming toxin. *Biochim. Biophys. Acta* **1780**, 612–618 (2008).
42. Matsuyama, A. *et al.* pDUAL, a multipurpose, multicopy vector capable of chromosomal integration in fission yeast. *Yeast* **21**, 1289–1305 (2004).
43. Gachet, Y. & Hyams, J.S. Endocytosis in fission yeast is spatially associated with the actin cytoskeleton during polarised cell growth and cytokinesis. *J. Cell Sci.* **118**, 4231–4242 (2005).

Acknowledgments

We thank C. Boone (Univ. Toronto) for sharing unpublished results and discussions, A. Fujie (Astellas Pharma) for kind gifts of FK463 and cispentacin, K. Takegawa (Kyushu Univ.) for *erg* deletion strains, T. Kuno (Kobe Univ.) for the *bgs1* mutant and *pck* deletion strains and K. Nakano (University of Tsukuba) for *rho1*-expression plasmids. We also thank J. Ishiguro (Konan Univ.) for the *act1/cps8* mutant strain, which was provided through the Yeast Genetic Resource Center (YGRC), N. Kanoh, S. Shimizu and H. Osada (RIKEN Advanced Science Institute) for helping in the preparation of TNM affinity beads, J. Ochi (Kyoto Univ.) for technical assistance and J. Piotrowski (RIKEN Advanced Science Institute) for critical reading of the manuscript. We are grateful to the RIKEN Brain Science Institute's Research Resource Center for mass spectrometry. This work was supported in part by the New Energy and Industrial Technology Development Organization Project on Development of Basic Technology to Control Biological Systems Using Chemical Compounds, a Grant-in-Aid from the Ministry of Education, Culture, Sports, Science and Technology of Japan and the Chemical Genomics Research Project, RIKEN Advanced Science Institute.

Author contributions

M.Y. is responsible for project planning and experimental design, with support from K.I., H. Kawasaki, H. Kakeya and T.K.; S.N. performed most of the experiments; Y.A. assisted *in vitro* sterol binding experiments; M.H. assisted chemical-genomic screen; A.M. and A.S. prepared the yeast strain collection; S.M. prepared theonellamides.

Competing financial interests

The authors declare no competing financial interests.

Additional information

Supplementary information, chemical compound information and chemical probe information is available online at http://www.nature.com/naturechemicalbiology/. Reprints and permissions information is available online at http://npg.nature.com/reprintsandpermissions/. Correspondence and requests for materials should be addressed to M.Y.

Inhibition of translation by cytotrienin A—a member of the ansamycin family

LISA LINDQVIST,[1] FRANCIS ROBERT,[1] WILLIAM MERRICK,[2] HIDEAKI KAKEYA,[3] CHRISTOPHER FRASER,[4] HIROYUKI OSADA,[5] and JERRY PELLETIER[1,6]

[1]Department of Biochemistry, McGill University, Montreal, Quebec H3G 1Y6, Canada
[2]Department of Biochemistry, School of Medicine, Case Western Reserve University, Cleveland, Ohio 44106, USA
[3]Department of System Chemotherapy and Molecular Sciences, Graduate School of Pharmaceutical Sciences, Kyoto University, Kyoto 606-8501, Japan
[4]Department of Molecular and Cellular Biology, UC Davis, University of California, Davis, California 95616, USA
[5]Chemical Biology Department, Advanced Science Institute, RIKEN, Wako-shi, Saitama 351-0198, Japan
[6]The Rosalind and Morris Goodman Cancer Centre, McGill University, Montreal, Quebec H3G 1Y6, Canada

ABSTRACT

The ansamycins are a diverse and often physiologically active group of compounds that include geldanamycin and rifamycin, inhibitors of heat shock protein 90 and prokaryotic DNA-dependent RNA synthesis, respectively. Cytotrienin A is an ansamycin-type small molecule with potent antiproliferative and proapoptotic properties. Here, we report that this compound inhibits eukaryotic protein synthesis by targeting translation elongation and interfering with eukaryotic elongation factor 1A function. We also find that cytotrienin A prevents HUVEC tube formation and diminishes microvessel formation in the chorioallantoic membrane assay. These results provide a molecular understanding into cytotrienin A's previously reported properties as an anticancer apoptosis-inducing drug.

Keywords: cytotrienin A; eEF1A; translation inhibitor; protein synthesis

INTRODUCTION

There is much interest in identifying and characterizing novel inhibitors of eukaryotic protein synthesis, both as tools to characterize the translation machinery and as drugs that can curtail malignant cell proliferation (Pelletier and Peltz 2007). There are several observations that suggest a high therapeutic index can be achieved by inhibiting translation in cancers. One vulnerability of cancer cells is at the level of ribosome recruitment, where mRNAs must compete with each other for limiting amounts of translation initiation factors (Duncan et al. 1987). Translation of mRNAs that are "weak" competitors for eukaryotic initiation factors (eIFs) are therefore more sensitive to small changes in the levels of these factors. Since several of the "weak" mRNAs characterized to date encode for antiapoptotic or prosurvival factors, their selective down-regulation preferentially curtails growth of tumor cells in preclinical cancer models (Graff et al. 2007; Cencic et al. 2009; Lucas et al. 2009). In addition, translation initiation inhibitors have been shown to exert antiangiogenic activities, a property that may contribute to their anti-cancer activity (Graff et al. 2007; Cencic et al. 2009). Additionally, the rapid reduction in levels of pro-oncogenic and pro-survival proteins having short half-lives (Chao et al. 1998; Nijhawan et al. 2003) occurs upon translation inhibition, and this can impair the growth of transformed cells. Higher translation rates also occur in human tumors and appear to be required to maintain their oncogenic state (Heys et al. 1991; Wendel et al. 2004). These latter two points may explain why some inhibitors of translation elongation show efficacy in preclinical cancer models as well as in the clinic (Quintas-Cardama et al. 2009; Robert et al. 2009).

The first step of translation elongation is catalyzed by eukaryotic elongation factor (eEF) 1A, which delivers the aminoacyl-tRNA (aa-tRNA) to the ribosomal A site, followed by GTP hydrolysis (provided that the proper codon–anticodon interaction occurs). There are two isoforms of eEF1A, eEF1A1 and eEF1A2, which are encoded by separate genes and show 95% identity. Both isoforms are thought to

Reprint requests to: Jerry Pelletier, McIntyre Medical Sciences Building, Room 810, 3655 Promenade Sir William Osler, McGill University, Montreal, Quebec H3G 1Y6, Canada; e-mail: jerry.pelletier@mcgill.ca; fax: (514) 398-7384.

Article published online ahead of print. Article and publication date are at http://www.rnajournal.org/cgi/doi/10.1261/rna.2307710.

be functionally redundant for translation, although they are differentially expressed (Kahns et al. 1998) and both have been shown capable of acting as oncogenes in the appropriate setting (Thornton et al. 2003).

Here, we describe the characterization of a novel modulator of eEF1A from the ansamycin family. Cytotrienin A (Cyt A) is a natural product produced by *Streptomyces* sp., which has been previously reported to induce apoptosis in leukemia cell lines by activating c-Jun N-terminal kinase (JNK), p38 mitogen-activated protein kinase (MAPK), and p36 myelin basic protein (MBP) kinase (Kakeya et al. 1998; Watabe et al. 2000). Here, we report that Cyt A inhibits translation elongation by interfering with eEF1A function. Our results provide molecular insight into Cyt A's previously reported properties as an anti-cancer compound.

RESULTS

Cytotrienin A inhibits translation elongation

During the course of a high-throughput screen to identify translation inhibitors (Novac et al. 2004), Cyt A (Fig. 1A) was identified as a "hit" that inhibited both cap-dependent (Firefly [FF] luciferase) and hepatitis C virus (HCV)-driven (*Renilla* [Ren] luciferase) translation in Krebs-2 extracts

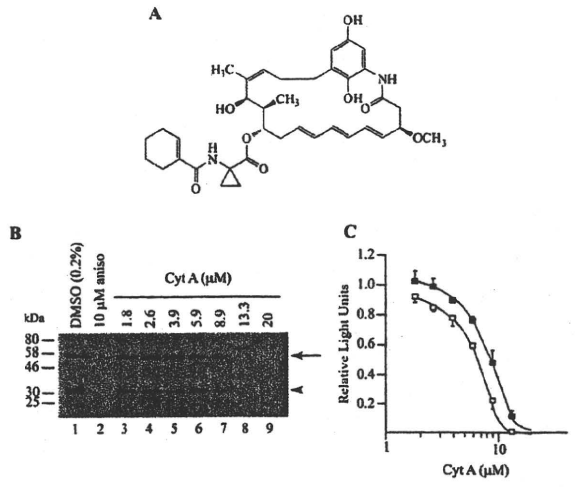

FIGURE 1. Cyt A inhibits eukaryotic translation. (*A*) Chemical structure of Cyt A. (*B*) Cyt A inhibits both cap-dependent and HCV IRES-driven translation in Krebs-2 extracts. In vitro translations were performed in the presence of [^{35}S]methionine and programmed with FF/HCV/Ren. DMSO, anisomycin (aniso), or Cyt A (lanes *3–9*) were added to Krebs-2 extracts at the indicated concentrations. Proteins were separated by SDS-PAGE and visualized by autoradiography. The arrow and arrowhead denote Firefly and *Renilla* luciferase, respectively. (*C*) Luciferase activity from translations performed in Krebs-2 extracts programmed with FF/HCV/Ren shown in *B*. Light units were set relative to the values obtained in the presence of vehicle (DMSO). The average of three measurements is shown with the SEM represented by error bars.

(Fig. 1B,C) and in rabbit reticulocyte lysate (RRL) (data not shown). Cyt A was also active in wheat-germ extracts, but did not significantly inhibit prokaryotic translation in *E. coli* S30 extracts at 50 μM (data not shown). These results indicate that Cyt A inhibits both cap-dependent and IRES-dependent translation. To determine whether the initiation phase of translation was affected by Cyt A, we performed ribosome binding experiments to assess the effects of Cyt A on 80S complex formation (Fig. 2A). Cyt A was able to stabilize 80S complexes to a similar degree as cycloheximide (CHX) (Fig. 2A, left and right panels, respectively). As well, addition of the initiation inhibitor hippuristanol, followed by addition of Cyt A to the binding reactions, caused a decrease in 80S complex formation (Fig. 2A, left), similar to if Hipp alone was present in the binding reactions (Fig. 2A, right). However, if Cyt A was present in the extract prior to the addition of Hipp, 80S complexes were trapped to the same efficiency as observed for Cyt A (Fig. 2A, left). Consistent with these results, Cyt A inhibited the translation of poly(Phe) from poly(U) RNA (Fig. 2B). Taken together, these experiments strongly suggest that Cyt A targets translation elongation.

The elongation inhibitors homoharringtonine (HHT) and bruceantin (Bru) inhibit only newly initiated ribosomes during the first step of elongation and allow translating ribosomes to run-off mRNA templates (Pelletier and Peltz 2007; Robert et al. 2009). To determine whether Cyt A showed similar properties, we performed in vitro translation reactions in the presence of [^{35}S]methionine, where compound was added 5 min after the start of translation (Fig. 2C). A kinetic analysis was performed to quantitate the amount of product synthesized. Inhibition of translation by HHT is delayed by several minutes following its addition to a translating extract as polysomes run-off mRNA templates due to the reduced affinity of HHT for actively translating ribosomes (Fig. 2C; Chan et al. 2004). Addition of Cyt A immediately inhibited protein synthesis in a manner similar to CHX. These results indicate that Cyt A affects translating ribosomes and does not allow polysome run-off.

Cyt A modulates eEF1A-dependent aa-tRNA binding to the ribosome

To better understand the mechanism by which Cyt A inhibits elongation, we analyzed its effects on tRNA binding to the ribosome, peptide bond formation, and translocation. We first tested whether Cyt A could inhibit the peptidyl transferase activity of the ribosome by monitoring the formation of [^{35}S]methionyl-puromycin. Cyt A did not inhibit peptidyl transferase activity under these conditions, unlike the known peptdyl transferase inhibitor HHT (Fig. 3A).

We next assessed whether Cyt A could affect binding of aa-tRNA to ribosomes in eEF1A-independent [high poly(U)

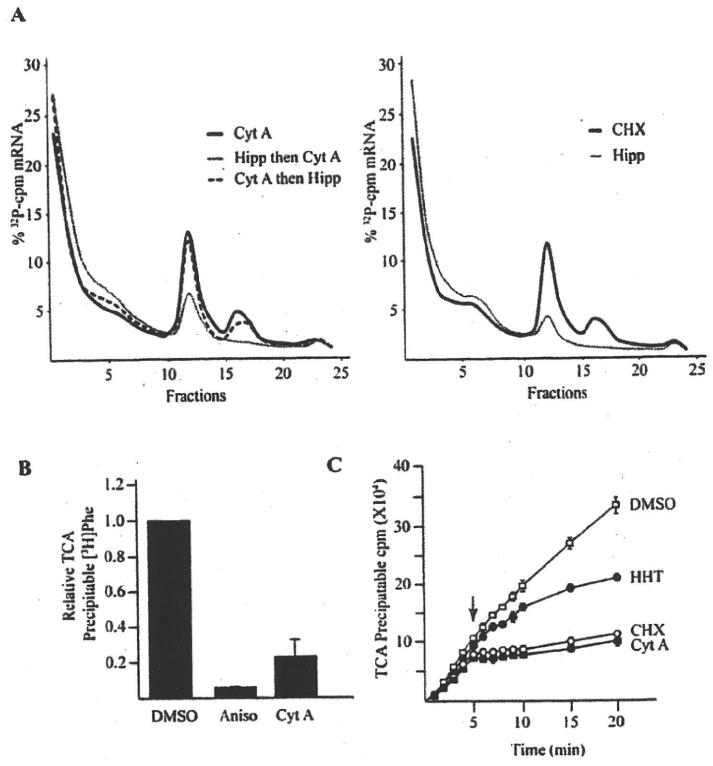

FIGURE 2. Cyt A inhibits translation elongation. (*A*) Cyt A does not inhibit translation initiation. Ribosome bindings were performed in RRL using ^{32}P-labeled CAT RNA. Reactions were separated by centrifugation on 10%–30% glycerol gradients and fractions quantitated by scintillation counting. (*Left*) Ribosome bindings were performed in the presence of 50 μM Cyt A alone, preincubated with 50 μM hippuristanol (Hipp), followed by addition of 50 μM Cyt A, or preincubated with 50 μM Cyt A, followed by the addition of 50 μM Hipp. (*Right*) Ribosome bindings were performed in the presence of 0.6 mM CHX or 50 μM Hipp. Both panels are part of the same experiment, but were separated for clarity. (*B*) Cyt A inhibits translation elongation. In vitro translations in RRL supplemented with [^{3}H]phenylalanine and programmed with poly(U) RNA. Polypeptides were TCA precipitated and quantitated by scintillation counting. Counts were set relative to DMSO levels. The average of four measurements is shown with the SEM. (*C*) Cyt A does not permit ribosome run-off. In vitro translation reactions of Krebs-2 extracts were allowed to proceed in the absence of compound for 5 min, after which time DMSO, HHT (200 μM), CHX (50 μM), or Cyt A (20 μM) were added. Aliquots were taken at the indicated times, TCA precipitated, and quantitated by scintillation counting. The average of three measurements is shown with the SEM. The downward arrow indicates the point of addition of compound or vehicle.

RNA concentration] or eEF1A-dependent [low poly(U) RNA concentration] reconstituted systems. The ability of [^{14}C]Phe-tRNA^{Phe} to bind ribosomes was not affected by Cyt A when binding was eEF1A independent (Fig. 3B), indicating that Cyt A does not compete with [^{14}C]Phe-tRNA^{Phe} for the ribosome. Under eEF1A-dependent conditions, the levels of ribosome-bound [^{14}C]Phe-tRNA^{Phe} in the presence of GDP or GMPPNP were similar to those binding reactions lacking eEF1A in DMSO controls (Fig. 3C). [Also note that tRNA binding without eEF1A in this experiment is much lower than in the experiment presented in Fig. 3B, due to a 1000-fold decrease in poly(U) RNA template.] In the presence of GTP, the amount of [^{14}C]Phe-tRNA^{Phe} bound to ribosomes increased significantly (Fig. 3C). Under this condition, both Cyt A and CHX decreased [^{14}C]Phe-tRNA^{Phe} binding by ~40%, while Did B had no significant effect. The low amount of [^{14}C]Phe-tRNA^{Phe} binding to ribosomes observed in the presence of GMPPNP was increased when either Cyt A or Did B was present in the reactions (Fig. 3C). One interpretation of this result is that Cyt A stabilizes the ternary complex on the ribosome (see Discussion).

eEF2-dependent translocation is inhibited by Cyt A only when aa-tRNA is delivered in an eEF1A-dependent manner

The ability of Cyt A to affect eEF2-dependent translocation was also investigated. After either nonenzymatic (as in Fig. 3B) or eEF1A-dependent aa-tRNA binding to the ribosome (with GTP, as in Fig. 3C), translocation was initiated by the addition of puromycin and eEF2. Under these conditions, CHX inhibited translocation regardless of whether [^{14}C]Phe-tRNA^{Phe} binding was eEF1A dependent or eEF1A independent, whereas Cyt A inhibited translocation only when charged tRNA was loaded in an eEF1A-dependent manner (Fig. 3D). Did B served as a positive control in the eEF1A-dependent translocation assay and was found to inhibit this reaction (Fig. 3D).

Cyt A inhibits neither ternary complex formation nor the GTPase activity of eEF1A

The inhibitory effect in the presence of GTP and stimulatory effect in the presence of GMPPNP of Cyt A on tRNA binding could result from improper ternary complex formation (eEF1A:GTP:aa-tRNA). To determine whether Cyt A affects the ability of eEF1A to bind to GTP, we performed a UV cross-linking experiment with [α-^{32}P]GTP in the presence or absence of Phe-tRNA^{Phe} (Fig. 4A). We observed no significant change in the efficiency of GTP cross-linking to eEF1A in the presence of Cyt A (Fig. 4A, cf. lanes 2 and 5 with 1 and 4, respectively). Excess GTP competed for the radiolabeled [α-^{32}P]GTP in this assay (cf. lane 3 and 6 with 1 and 4, respectively). As well, Cyt A did not prevent eEF1A:[^{14}C]-Phe-tRNA^{Phe} complex formation, as assessed by electrophoretic mobility shift assay (EMSA) (Fig. 4B). We investigated

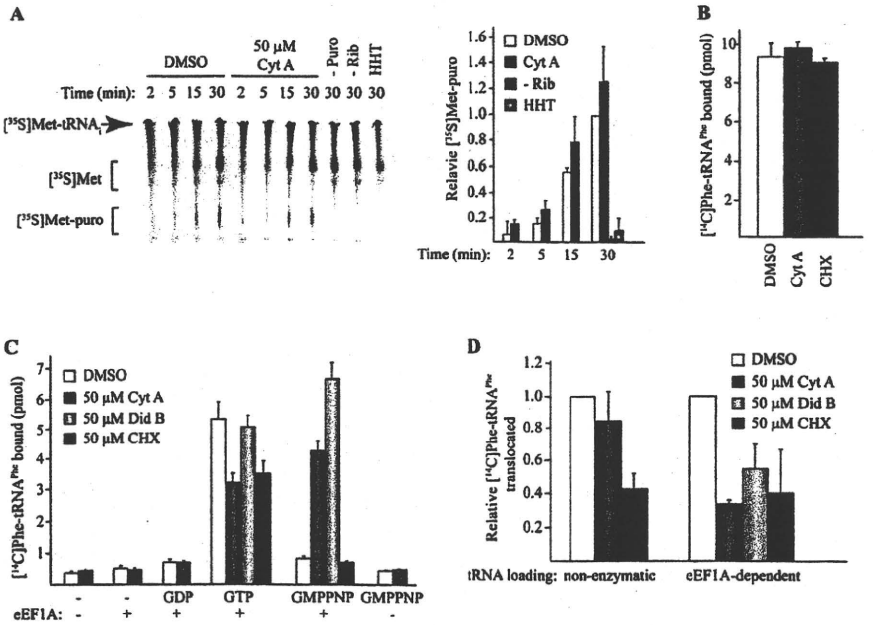

FIGURE 3. The effect of Cyt A on the steps of translation elongation. (*A*) Cyt A does not inhibit peptidyl transferase activity. [^{35}S]Methionine-puromycin formation was monitored in the presence of purified 40S and 60S ribosomes using [^{35}S]Met-tRNA$_i$ and ribosomal high-salt wash from RRL. (*Left*) Aliquots of samples were taken at the indicated time points and separated by TLC. The position of migration of [^{35}S]Met-puro, [^{35}S]Met, and [^{35}S]Met-tRNA$_i$ is indicated to the *left*. The addition of 50 μM Cyt A, 40 μM HHT, or the absence of puromycin (−Puro) or ribosomes (−Rib) is indicated at *top*. (*Right*) Quantitation of [^{35}S]Met-puro production. The average of four experiments relative to the DMSO control at 30 min is shown. Note that values obtained from the reaction in the absence of puromycin were subtracted as background. The SEM is represented using error bars. (*B*) Cyt A does not inhibit eEF1A-independent [^{14}C]Phe-tRNA^{Phe} binding to 80S ribosomes. Filter binding of [^{14}C]Phe-tRNA^{Phe} was performed with purified 80S ribosomes, 0.4 mg/mL poly(U) RNA, and either DMSO, 50 μM Cyt A, or 50 μM CHX. The average of four experiments is shown with the SEM indicated by error bars. (*C*) Cyt A modulates eEF1A-dependent [^{14}C]Phe-tRNA^{Phe} binding to 80S ribosomes. Filter binding of [^{14}C]Phe-tRNA^{Phe} with purified 80S ribosomes, and 0.4 μg/mL poly(U) RNA in the presence of either DMSO, 50 μM Cyt A, 50 μM DidB, or 50 μM CHX. The presence of eEF1A and nucleotide is indicated. The average of three to six measurements is shown with SEM indicated by error bars. (*D*) eEF2-dependent translocation of [^{14}C]Phe-tRNA^{Phe} is inhibited by Cyt A only when aminoacyl-tRNA is loaded in an eEF1A-dependent manner. Following nonenzymatic or eEF1A-dependent tRNA binding (as described in *B* and *C* with GTP, respectively), eEF2 was added to the reaction with puromycin. The amount of puromycin-active [^{14}C]Phe-tRNA^{Phe} was extracted with ethyl aceteate and quantitated by scintillation counting. tRNA already bound to the P-site was subtracted from these values (see Materials and Methods) and set relative to the DMSO control. The average of two to four experiments is shown with the SD.

whether Cyt A affects the GTPase activity of eEF1A and found no evidence to this effect (Fig. 4C). We conclude that Cyt A does not interfere with ternary complex formation.

Cellular protein synthesis is inhibited by Cyt A

[^{35}S]Methionine/cysteine labeling of HeLa cells was inhibited by Cyt A, whereas DNA and RNA synthesis was not dramatically affected (Fig. 5A). Inhibition of translation was reversible and showed almost complete recovery by 6 h after removal of the compound (Fig. 5B). The polysome profile of cells exposed to Cyt A for 1 h showed a similar to slight increase in polysomes compared with those isolated from cells exposed to vehicle (DMSO) (Fig. 5C). When hippuristanol was added during the last 30 min of Cyt A treatment, polysomes were still present, unlike what was observed when cells were exposed to only hippuristanol (Fig. 5C, left). Cells treated with HHT, which is known to allow ribosome run-off, showed an absence of polysomes (Fig. 5C, right). This data is consistent with Cyt A causing stalling of translating ribosomes and allowing their accumulation on mRNA templates.

Antiangiogenic properties of Cyt A

Inhibition of translation has been shown to impair angiogenesis and has been suggested as a mechanism by which they function as anti-cancer therapeutics (Taraboletti et al. 2004; Graff et al. 2007; Cencic et al. 2009). We therefore tested whether Cyt A might have similar properties. To examine this, we utilized a HUVEC tube formation assay, which has been previously used to mimic some aspects of angiogenesis (Kubota et al. 1988; Graff et al. 2007; Cencic et al. 2009). The inhibition of tube formation with Cyt A was dose dependent (Fig. 6A,B) at concentrations where

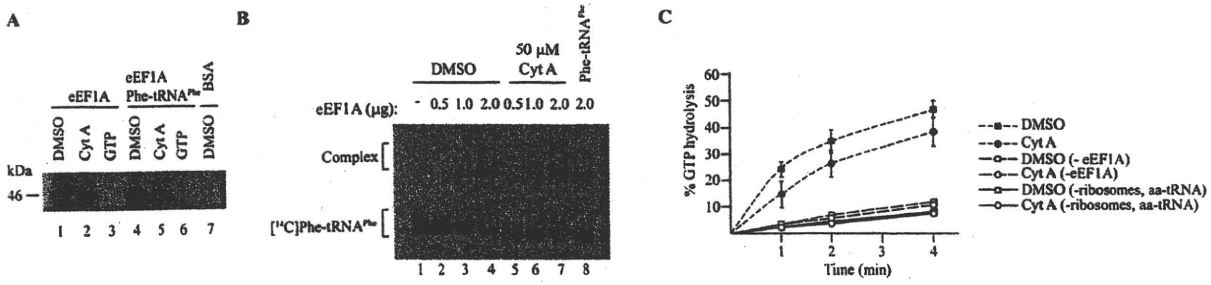

FIGURE 4. Cyt A does not affect ternary formation. (*A*) Cyt A does not inhibit GTP binding to eEF1A. Purified eEF1A (1 μg) was UV cross-linked to [α^{32}P]GTP in the presence (lanes *4–7*) or absence (lanes *1–3*) of Phe-tRNA^{Phe} and 50 μM Cyt A or 1 mM unlabeled GTP. Reactions were treated with RNase A, separated by SDS-PAGE, and visualized by autoradiography. (*B*) Cyt A does not affect [^{14}C]Phe-tRNA^{Phe} binding to eEF1A. Increasing amounts of eEF1A were incubated with [^{14}C]Phe-tRNA^{Phe} in the presence of DMSO, 50 μM Cyt A, or unlabeled Phe-tRNA^{Phe} competitor. EMSAs were performed on 6% polyacrylamide gels and visualized by autoradiography. The position of migration of free [^{14}C]Phe-tRNA^{Phe} and complexes are indicated to the *left*. (*C*) Cyt A does not affect the GTPase activity of eEF1A. eEF1A and [γ-^{32}P]GTP were incubated with 40S and 60S ribosomes and Phe-tRNA^{Phe} in the presence of 50 μM Cyt A or DMSO. GTPase activity was also measured in the absence of eEF1A or without ribosomes or Phe-tRNA^{Phe}. The average of three to four measurements is shown with the SEM represented as error bars.

general translation was inhibited by >90%, (Fig. 6C, open circles) similar to effects observed with silvestrol (Silv), a previously reported translation initiation inhibitor with antiangiogenic properties (Fig. 6A; data not shown) (Cencic et al. 2009). Importantly, cells remained viable under these conditions (Fig. 6C, squares). We also tested the ability of Cyt A to inhibit angiogenesis in the more physiological chorioallantoic membrane (CAM) assay. Cyt A inhibited new vessel growth in a dose-dependent manner (Fig. 6D), similar to the inhibitor of VEGF receptor tyrosine kinase Semaxanib (SU5416) (Riboldi et al. 2005).

DISCUSSION

Ansamycins form a diverse family of compounds exerting a number of physiological effects on mammalian and viral systems (Isaacs et al. 2003; Floss and Yu 2005). In this study, we identified a member of this family as an inhibitor of eukaryotic translation elongation. Other ansamycins such as rifabutin and 17-AAG did not inhibit protein synthesis in vitro in Krebs-2 extracts at 50 μM (data not shown), indicating that this is not a general property of this group of compounds.

Increasing evidence links deregulated protein synthesis and cancer growth (Lindqvist and Pelletier 2009). Indeed, two inhibitors of elongation (HHT and a derivative of Did B) have advanced to clinical trials (Le Tourneau et al. 2007; Quintas-Cardama et al. 2007). In addition, we have previously shown that inhibitors of elongation can sensitize select tumors to the pro-apoptotic properties of the clinical agent doxorubicin (Robert et al. 2009). Inhibition of translation could, in principle, suppress drug resistance by curtailing the synthesis of antiapoptotic proteins and/or drug transporters. Leukemic cell lines have been previously shown to be more sensitive to Cyt A-induced apoptosis compared with other tumor cell lines, supporting a potential therapeutic use of Cyt A in blood cancer treatment (Watabe et al. 2000). Here, we show that Cyt A inhibits protein synthesis in cell lines that were previously shown to be resistant to Cyt A-induced apoptosis (Fig. 5A) as well as in nontransformed HUVECs (Fig. 6C). Indeed HeLa, HUVEC, and Jurkat (a leukemia cell line previously shown to undergo apoptosis after a 24-h exposure to Cyt A [IC_{50} = 13.87 nM]; Watabe et al. 2000) cells all had very similar IC_{50}s with respect to translation inhibition (data not shown). These results suggest that the differential sensitivity of different cell lines to the apoptotic response is not due to a difference in sensitivity to Cyt A-induced protein synthesis inhibition but may depend on intrinsic factors that link the apoptotic response to the translation apparatus. We demonstrate that translation inhibition occurs well before apoptosis can be detected and, therefore, must precede the apoptotic response (Fig. 6C). The fact that Cyt A induces apoptosis more readily in leukemia is consistent with reports that B-cell and leukemia-cell lines also are more sensitive to the translation initiation inhibitor silvestrol compared with other cell types (Monks et al. 1991; Lucas et al. 2009).

Translation elongation can be inhibited in an eEF1A-dependent manner also by interfering with ternary complex formation (eEF1A:GTP:aminoacyl-tRNA). Indeed, several antibiotics target this step, including GE2770A and pulvomycin (Heffron and Jurnak 2000; Andersen et al. 2003). This mechanism is in contrast to that of Cyt A (Fig. 4A,B). Pulvomycin is known to increase the GTPase activity of EF-Tu, the bacterial homolog of eEF1A (Andersen et al. 2003), while both Did B and Cyt A do not alter GTPase activity of eEF1A to any significant extent (Fig. 4C; Crews et al. 1994; Ahuja et al. 2000). Therefore, the mechanism of action of Cyt A does not seem to be reminiscent of these EF-Tu-targeting inhibitors.

Cyt A stalled polyribosomes on mRNA templates and inhibited translating ribosomes, similar to what has been reported for the translation elongation inhibitors CHX and

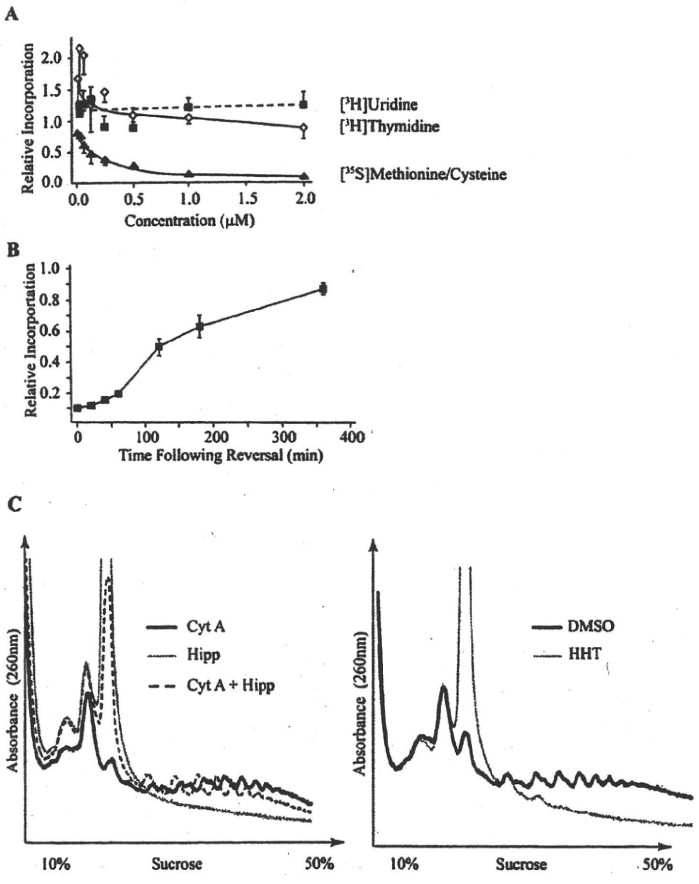

FIGURE 5. Cyt A reversibly inhibits translation in cell culture. (*A*) Consequences of Cyt A exposure on DNA, RNA, and protein synthesis in HeLa cells. Cyt A was added to cell medium for 1 h and [6-^{3}H]thymidine, [5-^{3}H]uridine, or [^{35}S]methionine/cysteine was present during the last 20 min of incubation. Counts from TCA-precipitated material were normalized to total protein content and set relative to the DMSO control. The average of four data points is shown with the SEM indicated by error bars. (*B*) Inhibition of translation by Cyt A is reversible. HeLa cells were incubated in 2 μM Cyt A for 1 h, after which fresh medium lacking Cyt A was added. Twenty minutes before lysis, [^{35}S]methionine/cysteine was added. Normalization was performed to total protein concentration and set relative to the DMSO control. The average of four measurements is shown with the SEM represented by error bars. (*C*) Cyt A does not allow ribosome run-off in cell culture. Polysome formation in HeLa cells exposed to 2 μM Cyt A for 1 h and/or 5 μM Hipp for 30 min or 0.5 μM HHT for 1 h. Panels are from the same experiment and were separated for clarity.

Did B (Fig. 5C; Urdiales et al. 1996; Schneider-Poetsch et al. 2010). In the eEF1A-dependent aa-tRNA-binding experiment (Fig. 3C), the amount of [^{14}C]Phe-tRNA^{Phe} bound to ribosomes was significantly reduced in the presence of GMPPNP compared with GTP (Fig. 3C). We believe this may be due to the large dilution (~100-fold) that occurs during processing of the samples for filter binding, allowing dissociation of the ternary complex from the ribosome. This is consistent with the finding that only after GTP hydrolysis is the charged tRNA locked in the A site (Rodnina and Wintermeyer 2001). Hence, one interpretation of our results is that in the presence of GMPPNP, the aa-tRNA is lost from the ribosome. However, this is not observed if Did B or Cyt A are present (Fig. 3C), suggesting that these compounds stabilize the aa-tRNA:ribosome interaction, perhaps by blocking release of eEF1A. Both Cyt A and Did B inhibited translocation when aa-tRNA was loaded in an eEF1A-dependent manner (Fig. 3D; SirDeshpande and Toogood 1995), which would be consistent with this model, since eEF2 and the ternary complex share binding sites on the ribosome (Marco et al. 2004). Indeed, this mode of action has been suggested for Did B previously and is the mechanism of action of the antibiotic kirromycin (Wolf et al. 1977; Ahuja et al. 2000; Andersen et al. 2003; Schmeing et al. 2009). It remains to be determined whether Cyt A binds directly to the ribosome and/or to eEF1A.

It has recently been suggested that tumor reduction caused by eIF4F inhibition may partially be caused by inhibiting angiogenesis (Graff et al. 2007; Cencic et al. 2009). Here, we show that Cyt A can also inhibit angiogenesis as Cyt A-inhibited HUVEC tube formation (Fig. 6A,B) as well as microvessel development in the CAM assay (Fig. 6D) in a manner similar to Did B (Taraboletti et al. 2004). These results suggest that Cyt A merits further study, not only for hematological cancers, but also for solid tumors requiring angiogenesis for optimal growth.

MATERIALS AND METHODS

Materials

Cyt A was prepared as previously described and stored in 100% DMSO (Kakeya et al. 1997). Didemnin B (Did B) (NCI-Developmental Therapeutics Program), homoharringtonine (HHT) (Sigma-Aldrich), and cycloheximide (CHX) (Bioshop) were stored in 100% DMSO, whereas anisomycin (Sigma) was resuspended in H_2O. Hippuristanol was purified as previously described (Bordeleau et al. 2006). All compounds were stored at −80°C.

Cell culture experiments

HeLa cells were grown in DMEM containing 10% fetal bovine serum and 100 U/mL penicillin/streptomycin. HUVEC cells (Lonza Walkersville, Inc.) were grown in EMB-2 medium supplemented with EGM-2.

For thymidine labeling of DNA, cells were serum starved for 48 h, followed by the addition of serum for 7 h, at which point

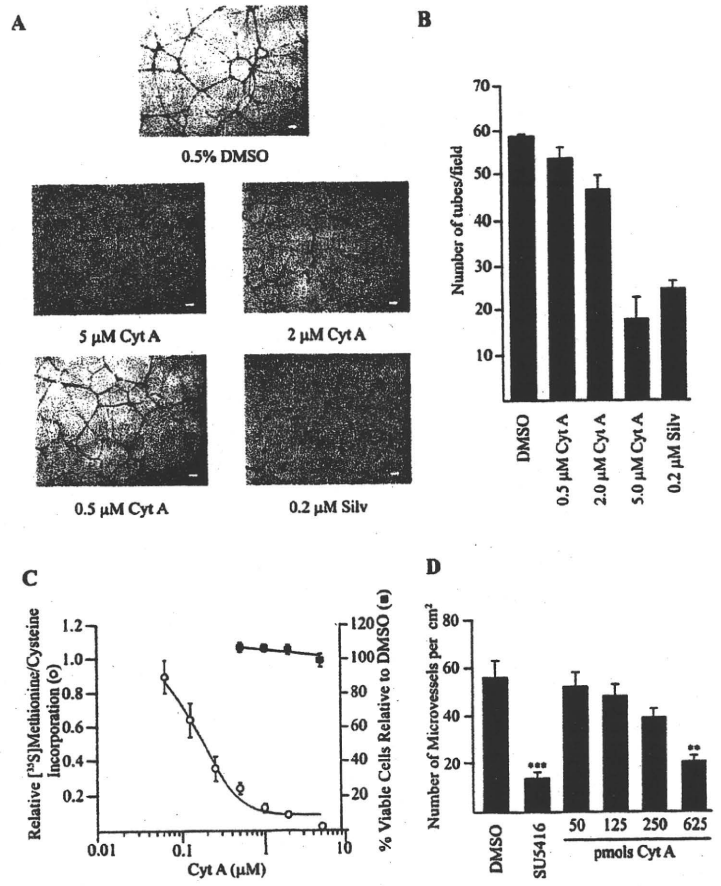

FIGURE 6. Cyt A inhibits angiogenesis. (*A*) Photomicrographs of HUVEC tube formation at different concentrations of Cyt A or silvestrol (Silv). Scale bar, 0.1 mm. (*B*) Quantitation of tube formation in HUVECs. Each well was photographed in seven fields, and the average number of tubes formed was counted. The average of four experiments is shown. Error bars represent the SEM. (*C*) Cyt A inhibits protein synthesis without inducing apoptosis in HUVECs. Following a 24-h exposure to Cyt A or DMSO, HUVECs were labeled for 20 min with [^{35}S]methionine/cysteine or monitored for apoptosis. For the translation assays, TCA-precipitable material was normalized to total protein content and set relative to the DMSO control. The average of four measurements is shown with the SEM represented by error bars. Cell viability was judged by the relative percent of Annexin-FITC or propidium iodide staining compared with DMSO controls. The average of five data points is shown with the SEM represented by error bars. (*D*) Cyt A inhibits angiogenesis in the CAM assay. Values presented represent the average number of vessels per cm^2 area for three samples with the SEM; $^{**}P < 0.01$ (vs. vehicle); $^{***}P < 0.001$ (vs. vehicle).

compound was added for 1 h. [6-^{3}H]thymidine (10 Ci/mmol) (Perkin Elmer) was present for the last 20 min of the reaction. For RNA labeling, cells were not serum starved and [5-^{3}H]uridine (26.3 Ci/mmol) (Perkin Elmer) was present during the last 20 min of a 1-h compound treatment. Cells were washed in PBS and lysed in RIPA buffer (50 mM Tris-HCl at pH 7.5, 150 mM NaCl, 1% NP-40, 0.5% sodium deoxycholate, 0.1% SDS). Radioactive incorporation was measured by TCA precipitation (5% TCA) onto GF/C filters (preblocked with 5% TCA and 0.1 M inorganic pyrophosphate). Filters were washed with 5 mL of cold 1% TCA, followed by 5 mL 100% ethanol, and quantified by scintillation counting. Counts were standardized to total protein content that had been determined using the D_c protein assay (Bio-Rad).

To monitor protein synthesis, cells were seeded into a 24-well dish and exposed to compound for 1 h with labeling performed during the last 20 min using [^{35}S]Easy Tag Express Protein Labeling mix (1175 Ci/mmol) (Perkin Elmer). Cells were lysed in RIPA buffer and an aliquot processed for TCA precipitation as described above.

HUVEC tube formation assays were performed as published previously (Cencic et al. 2009). HUVECs were seeded at 100,000 cell/well in the presence of compound on top of 300 μL of solidified BD Matrigel Matrix (BD Biosciences) in a 24-well dish. After 24 h, pictures were taken using a Nikon Eclipse TE300 microscope.

In vitro translation assays

In vitro translations were performed as previously reported (Novac et al. 2004). Translations were performed using a capped bicistronic mRNA reporter FF/HCV/Ren transcribed from pSP/(CAG)$_{33}$/FF/HCV/Ren.pA$_{51}$, in which firefly (FF) luciferase protein is produced by cap-dependent translation and *Renilla* (Ren) luciferase protein is generated by Hepatitis C virus (HCV) IRES-mediated initiation. Translation extracts were programmed with 8 μg/mL mRNA.

Experiments analyzing the consequences of Cyt A on actively translating ribosomes were performed in Krebs-2 extracts in the absence of in vitro-transcribed RNA, but in the presence of [^{35}S]methionine (Perkin Elmer), with compound being added 5 min after translation had been initiated. Aliquots (10 μL) were taken at the indicated times and added to 1.1 μL of 0.5 mM cycloheximide (CHX) and placed on dry ice to stop the reaction. Reactions were spotted onto 3 MM Whatman paper that had been preblocked with 50× amino acid mix (GIBCO). Filters were incubated in 10% TCA + 0.1% methionine on ice for 20 min, boiled in 5% TCA for 15 min, washed with 100% ethanol, dried, and the radioactivity quantitated by scintillation counting.

In vitro translation of poly(Phe) was performed in RRL using 50% RRL (Promega), 40 μM amino acid mix lacking phenylalanine, 40 μM methionine, 0.1 μg/μL poly(U) RNA, 4 μM magnesium acetate, 50 μM potassium acetate, and 50 μCi/mL [^{3}H]phenylalanine (Perkin Elmer). Following a 1-h incubation at 30°C, reactions were processed for TCA precipitation as described above.

Ribosome-binding assays and polysome profiling

Ribosome-binding assays were performed essentially as described previously (Robert et al. 2006). Briefly, compound was preincubated

with RRL at a final KCl concentration of 150 mM for 5 min, after which ^{32}P-labeled CAT mRNA was included. When a second compound was added, it was delivered 3 min after addition of RNA and reactions allowed to proceed at 30°C for 10 min. Reactions were centrifuged through a 10%–30% glycerol gradient at 39,000 rpm for 3.5 h in a SW40 rotor. Fractions (0.5 mL) were collected and quantitated by Cherenkov counting.

Polysome profiles of HeLa cells where visualized by treating cells with DMSO, 2 μM Cyt A, or 0.5 μM HHT for 1 h in a 10-cm^2 dish. Hippuristanol (5 μM) was added during the remaining 30 min. Cells were then washed in PBS containing 0.1 mg/mL CHX, scraped, and lysed in hypotonic lysis buffer (5 mM Tris-HCl at pH 7.5, 2.5 mM $MgCl_2$, 1.5 mM KCl, 0.1 mg/mL CHX, 2 mM DTT). The lysate was supplemented with 0.5% Triton X-100 and 0.5% sodium deoxycholate, centrifuged briefly (12,000*g* for 2 min), and the supernatant loaded onto 10%–50% sucrose gradients (20 mM HEPES-KOH at pH 7.5, 100 mM KCl, 5 mM $MgCl_2$, 1 mM DTT). Samples were centrifuged at 35,000 rpm for 2 h in a SW40 rotor at 4°C. The OD_{260} was monitored with a UA-6 UV detector (ISCO) using a Brandel tube piercer. Data was recorded using InstaCal Version 5.70 and TracerDaq Version 1.9.0.0 (Measurement Computing Corporation).

Peptidyl transferase assays

The peptidyl transferase assay was performed as previously described (Lorsch and Herschlag 1999). Briefly, [^{35}S]methionyl-$tRNA_i$ was generated by incubating 0.25 mg/mL total calf liver tRNA (Novogen) with 10 mM ATP, 10 mM CTP, 0.25 mg/mL leucovorin, 1 mCi/mL [^{35}S]methionine, and 0.875 μg/mL *E. coli* aminoacyl-tRNA synthetases (Sigma) in 50 mM sodium cacodylate (pH 7.4), 15 mM $MgCl_2$, and 7 mM 2-mercaptoethanol at 37°C for 30 min (Stanley 1974). Charged tRNA was purified by phenol/chloroform extraction, exclusion chromatography on a Sephadex G-50 spin-column, and ethanol precipitation.

Purified 40S and 60S ribosomes (0.06 μM) (Fraser et al. 2007), 0.5 mM GTP, 1 μM model RNA (GGAA[UC]$_7$UAUG[CU]$_{10}$C), 2 nM labeled [^{35}S]methionyl-$tRNA_i$, and a high-salt wash of ribosomes (Lorsch and Herschlag 1999) were incubated with 50 μM Cyt A. Reactions were subsequently started by the addition of 0.4 mM puromycin at 26°C. Aliquots were stopped in 0.4 M sodium acetate, spotted on cation-exchange IONEX-25 SA-Na TLC plates (Macherey-Nagel) (prerun in distilled water and dried), and developed in 2 M ammonium acetate and 10% acetonitrile. Experiments were visualized by phosphorimaging (Typhoon Trio, Amersham).

tRNA-binding and translocation assays

tRNA-binding and translocation assays were performed essentially as described (SirDeshpande and Toogood 1995; Robert et al. 2006). [^{14}C]Phe-tRNA^{Phe} was prepared by charging 0.2 mg/mL yeast tRNA^{Phe} (Sigma) with 3.75 mM ATP, 0.06 mM [^{14}C]phenylalanine in 50 mM Tris-HCl at pH 7.5, 20 mM $Mg(OAc)_2$, and 120 mM KCl using 10% (v/v) yeast S100 as the source of tRNA synthetase. Charged tRNA was purified via phenol/chloroform extraction, passed through a Sephadex G-50 spin-column, followed by ethanol precipitation (Odom et al. 1990).

For eEF1A-dependent assays, reactions were performed with 1.77 μM salt-washed 80S ribosomes, (0.4 μg/mL) poly(U) RNA, and 0.2 μM [^{14}C]Phe-tRNA^{Phe} with 4.65 μg of eEF1A. Either 0.15 mM GMP-PMP, GDP, or GTP was added in HEPES buffer (20 mM HEPES at pH 7.5, 10 mM $MgCl_2$, 100 mM KCl, 1 mM DTT) and reactions (100 μL) were incubated at 37°C for 30 min. Aliquots (6% of the total reaction) were taken, diluted in 0.8 mL of HEPES buffer and filtered through Type HA nitrocellulose filters (Millipore). Amino acyl-tRNA binding was quantitated by scintillation counting and values obtained without ribosomes were subtracted to remove background. The remaining reaction volume (of samples containing GTP) was used to perform translocation assays. Additional GTP (1 mM) was added to 15% of the samples in the presence or absence of 0.5 mM puromycin and/or 0.05 μg/μL eEF2 and incubated at 37°C for 30 min. The reaction was quenched with 1 M NH_4HCO_3 and extracted with ethyl acetate. Ninety percent of the organic layer was used for quantitation by scintillation counting. A puromycin assay was performed on 10% of the original reaction to determine the amount of aminoacyl-tRNA already bound to the P-site (Wurmbach and Nierhaus 1979), which was normalized and deducted from the values obtained above to determine the total amount of tRNA translocated.

Nonenzymatic tRNA-binding reactions were performed essentially as described for eIF1A, except higher amounts of poly(U) RNA (0.4 mg/mL) were used, and the reaction was performed in the absence of both GTP (or its analogs) and eEF1A. Reactions were carried out in Tris reaction buffer (50 mM Tris-HCl at pH 7.5, 60 mM KCl, 20 mM $MgCl_2$) containing 50 μM of compound. Translocation assays were performed as described above, except that they were carried out in Tris reaction buffer.

eEF1A enzymatic assays

GTP cross-linking to eEF1A was performed in 20-μL reactions containing 1 μg of eEF1A and 2.5 μCi of [α-^{32}P]GTP (3000 Ci/mmol) (Perkin Elmer) with or without 0.8 μg of Phe-tRNA^{Phe} (Sigma) in GTPase buffer (25 mM HEPES at pH 7.5, 125 mM KCl, 8.5 mM $MgCl_2$, 1 mM DTT). Reactions were incubated at 37°C for 15 min in the presence of 50 μM Cyt A, 1 mM cold GTP competitor, or DMSO, and cross-linked using a 254-nm germicidal UV lamp at 4°C for 15 min. Reactions were digested with 0.5 μg/μL RNase A for 10 min at 37°C, separated by SDS-PAGE, and visualized by autoradiography. Negative controls contained 1 μg of BSA instead of eEF1A.

Electrophoretic mobility shift assays were performed in 10-μL reactions in GTPase buffer using 0.5–2 μg of eEF1A and 1 mM GTP. Reactions were preincubated at room temperature for 10 min, after which time 20,000 cpm of [^{14}C]Phe-tRNA^{Phe} was added, and the incubation continued for an additional 15 min. Equivalent molar amounts of unlabeled Phe-tRNA^{Phe} were used as competitor. Reactions were analyzed on 6% native polyacrylamide (29:1 acrylamide:bisacrylamide) gels and electrophoresis performed in 1× TBE (90 mM Tris, 90 mM boric acid, 2 mM EDTA). Gels were then treated with En^{3}Hance (Perkin Elmer), washed in water, dried, and visualized by autoradiography.

GTPase assays (20 μL) were performed in GTPase buffer containing 0.5 μg of eEF1A and 1 μCi of [γ-^{32}P]GTP (6000 Ci/mmol) (Perkin Elmer) incubated with or without 0.8 μg of unlabeled Phe-tRNA^{Phe}, 16.8 pmol 40S, and 60S ribosomal subunits, and 31.4 pmol poly(U) RNA at 25°C. Control reactions were also performed without eEF1A or using only eEF1A (without tRNA, ribosomes or

RNA). Aliquots (2 μL) were taken and reactions stopped in 2 μL of 25 mM EDTA on ice. PEI Cellulose F TLC plates (EMD Chemicals, Inc.) were spotted with a 1.5-μL sample and developed using 0.3 M NaH_2PO_4/1 M $LiCl_2$. TLCs were quantitated using phosphorimaging on a Typhoon Trio (Amersham).

Viability assays

Viability assays were performed using Annexin-FITC and propidium iodide (PI) staining. HUVECs were treated with compound for 24 h in a 24-well plate. Cells were washed in PBS and trypsinized. Cells, PBS washes, and cell culture medium were collected together and centrifuged at 610*g* for 5 min. Cell pellets were washed in PBS and resuspended in 35 μL Annexin V binding buffer (10 mM HEPES-NaOH at pH 7.5, 140 mM NaCl, 2.5 mM $CaCl_2$). PI (Sigma) to a final concentration of 5 μg/mL and 1.75 μL FITC Annexin V (BD Biosciences Pharmingen) were added to reactions and incubated at RT for 20 min in the dark. Samples were diluted by the addition of 200 μL of Annexin V binding buffer and analyzed on a Guava Easy Cyte Plus (Millipore). Each experiment included unstained, PI-only, and Annexin V-only controls.

Chorioallantoic membrane (CAM) assay

The CAM assay was performed by Links Biosciences, LLC. Fertilized eggs were placed in an egg incubator at 37°C and 50% humidity. After 6 d, the egg shell was cracked and gently opened. A 5 × 5-mm sterile filter paper square saturated with either 25 μL of compound (50, 125, 250, 625 pmol), 4.2 nmol SU5416 (Sugen, Inc.), or vehicle (2% DMSO in PBS) was placed in areas between vessels. After 48 h, the CAMs were isolated and fixed in methanol/acetone. Representative images were collected by photography to permit quantitative analysis of vessel density.

ACKNOWLEDGMENTS

We thank Isabelle Harvey for technical assistance and Dr. T. Martin Schmeing for critical reading of the manuscript and insightful comments. L.L. was supported by a NSERC Alexander Graham Bell (CGSD) fellowship. This work was supported by a grant from the Canadian Cancer Society Research Institute (#20066) to J.P. and a NIH grant (R01 GM092927) to C.F.

Received June 7, 2010; accepted September 17, 2010.

REFERENCES

Ahuja D, Vera MD, SirDeshpande BV, Morimoto H, Williams PG, Joullie MM, Toogood PL. 2000. Inhibition of protein synthesis by didemnin B: How EF-1α mediates inhibition of translocation. *Biochemistry* **39:** 4339–4346.

Andersen GR, Nissen P, Nyborg J. 2003. Elongation factors in protein biosynthesis. *Trends Biochem Sci* **28:** 434–441.

Bordeleau ME, Mori A, Oberer M, Lindqvist L, Chard LS, Higa T, Belsham GJ, Wagner G, Tanaka J, Pelletier J. 2006. Functional characterization of IRESes by an inhibitor of the RNA helicase eIF4A. *Nat Chem Biol* **2:** 213–220.

Cencic R, Carrier M, Galicia-Vazquez G, Bordeleau ME, Sukarieh R, Bourdeau A, Brem B, Teodoro JG, Greger H, Tremblay ML, et al. 2009. Antitumor activity and mechanism of action of the cyclopenta[*b*]benzofuran, silvestrol. *PLoS ONE* **4:** e5223. doi: 10.1371/journal.pone.0005223.

Chan J, Khan SN, Harvey I, Merrick W, Pelletier J. 2004. Eukaryotic protein synthesis inhibitors identified by comparison of cytotoxicity profiles. *RNA* **10:** 528–543.

Chao JR, Wang JM, Lee SF, Peng HW, Lin YH, Chou CH, Li JC, Huang HM, Chou CK, Kuo ML, et al. 1998. mcl-1 is an immediate-early gene activated by the granulocyte-macrophage colony-stimulating factor (GM-CSF) signaling pathway and is one component of the GM-CSF viability response. *Mol Cell Biol* **18:** 4883–4898.

Crews CM, Collins JL, Lane WS, Snapper ML, Schreiber SL. 1994. GTP-dependent binding of the antiproliferative agent didemnin to elongation factor 1 alpha. *J Biol Chem* **269:** 15411–15414.

Duncan R, Milburn SC, Hershey JW. 1987. Regulated phosphorylation and low abundance of HeLa cell initiation factor eIF-4F suggest a role in translational control. Heat shock effects on eIF-4F. *J Biol Chem* **262:** 380–388.

Floss HG, Yu TW. 2005. Rifamycin-mode of action, resistance, and biosynthesis. *Chem Rev* **105:** 621–632.

Fraser CS, Berry KE, Hershey JW, Doudna JA. 2007. eIF3j is located in the decoding center of the human 40S ribosomal subunit. *Mol Cell* **26:** 811–819.

Graff JR, Konicek BW, Vincent TM, Lynch RL, Monteith D, Weir SN, Schwier P, Capen A, Goode RL, Dowless MS, et al. 2007. Therapeutic suppression of translation initiation factor eIF4E expression reduces tumor growth without toxicity. *J Clin Invest* **117:** 2638–2648.

Heffron SE, Jurnak F. 2000. Structure of an EF-Tu complex with a thiazolyl peptide antibiotic determined at 2.35 Å resolution: Atomic basis for GE2270A inhibition of EF-Tu. *Biochemistry* **39:** 37–45.

Heys SD, Park KG, McNurlan MA, Calder AG, Buchan V, Blessing K, Eremin O, Garlick PJ. 1991. Measurement of tumour protein synthesis in vivo in human colorectal and breast cancer and its variability in separate biopsies from the same tumour. *Clin Sci* **80:** 587–593.

Isaacs JS, Xu W, Neckers L. 2003. Heat shock protein 90 as a molecular target for cancer therapeutics. *Cancer Cell* **3:** 213–217.

Kahns S, Lund A, Kristensen P, Knudsen CR, Clark BF, Cavallius J, Merrick WC. 1998. The elongation factor 1 A-2 isoform from rabbit: Cloning of the cDNA and characterization of the protein. *Nucleic Acids Res* **26:** 1884–1890.

Kakeya H, Zhang HP, Kobinata K, Onose R, Onozawa C, Kudo T, Osada H. 1997. Cytotrienin A, a novel apoptosis inducer in human leukemia HL-60 cells. *J Antibiot* **50:** 370–372.

Kakeya H, Onose R, Osada H. 1998. Caspase-mediated activation of a 36-kDa myelin basic protein kinase during anticancer drug-induced apoptosis. *Cancer Res* **58:** 4888–4894.

Kubota Y, Kleinman HK, Martin GR, Lawley TJ. 1988. Role of laminin and basement membrane in the morphological differentiation of human endothelial cells into capillary-like structures. *J Cell Biol* **107:** 1589–1598.

Le Tourneau C, Raymond E, Faivre S. 2007. Aplidine: A paradigm of how to handle the activity and toxicity of a novel marine anticancer poison. *Curr Pharm Des* **13:** 3427–3439.

Lindqvist L, Pelletier J. 2009. Inhibitors of translation initiation as cancer therapeutics. *Future Med Chem* **1:** 1709–1722.

Lorsch JR, Herschlag D. 1999. Kinetic dissection of fundamental processes of eukaryotic translation initiation in vitro. *EMBO J* **18:** 6705–6717.

Lucas DM, Edwards RB, Lozanski G, West DA, Shin JD, Vargo MA, Davis ME, Rozewski DM, Johnson AJ, Su BN, et al. 2009. The novel plant-derived agent silvestrol has B-cell selective activity in chronic lymphocytic leukemia and acute lymphoblastic leukemia in vitro and in vivo. *Blood* **113:** 4656–4666.

Marco E, Martin-Santamaria S, Cuevas C, Gago F. 2004. Structural basis for the binding of didemnins to human elongation factor eEF1A and rationale for the potent antitumor activity of these marine natural products. *J Med Chem* **47:** 4439–4452.

Monks A, Scudiero D, Skehan P, Shoemaker R, Paull K, Vistica D, Hose C, Langley J, Cronise P, Vaigro-Wolff A, et al. 1991.

Feasibility of a high-flux anticancer drug screen using a diverse panel of cultured human tumor cell lines. *J Natl Cancer Inst* **83:** 757–766.

Nijhawan D, Fang M, Traer E, Zhong Q, Gao W, Du F, Wang X. 2003. Elimination of Mcl-1 is required for the initiation of apoptosis following ultraviolet irradiation. *Genes Dev* **17:** 1475–1486.

Novac O, Guenier AS, Pelletier J. 2004. Inhibitors of protein synthesis identified by a high throughput multiplexed translation screen. *Nucleic Acids Res* **32:** 902–915.

Odom OW, Picking WD, Hardesty B. 1990. Movement of tRNA but not the nascent peptide during peptide bond formation on ribosomes. *Biochemistry* **29:** 10734–10744.

Pelletier J, Peltz SW. 2007. Therapeutic Opportunities in Translation. In *Translational Control in Biology and Medicine*, (ed. MB Mathews et al.), pp. 855–895. Cold Spring Harbor Laboratory Press, Cold Spring Harbor, NY.

Quintas-Cardama A, Kantarjian H, Garcia-Manero G, O'Brien S, Faderl S, Estrov Z, Giles F, Murgo A, Ladie N, Verstovsek S, et al. 2007. Phase I/II study of subcutaneous homoharringtonine in patients with chronic myeloid leukemia who have failed prior therapy. *Cancer* **109:** 248–255.

Quintas-Cardama A, Kantarjian H, Cortes J. 2009. Homoharringtonine, omacetaxine mepesuccinate, and chronic myeloid leukemia circa 2009. *Cancer* **115:** 5382–5393.

Riboldi E, Musso T, Moroni E, Urbinati C, Bernasconi S, Rusnati M, Adorini L, Presta M, Sozzani S. 2005. Cutting edge: Proangiogenic properties of alternatively activated dendritic cells. *J Immunol* **175:** 2788–2792.

Robert F, Gao HQ, Donia M, Merrick WC, Hamann MT, Pelletier J. 2006. Chlorolissoclimides: New inhibitors of eukaryotic protein synthesis. *RNA* **12:** 717–725.

Robert F, Carrier M, Rawe S, Chen S, Lowe S, Pelletier J. 2009. Altering chemosensitivity by modulating translation elongation. *PLoS ONE* **4:** e5428. doi: 10.1371/journal.pone.0005428.

Rodnina MV, Wintermeyer W. 2001. Fidelity of aminoacyl-tRNA selection on the ribosome: Kinetic and structural mechanisms. *Annu Rev Biochem* **70:** 415–435.

Schmeing TM, Voorhees RM, Kelley AC, Gao YG, Murphy FV IV, Weir JR, Ramakrishnan V. 2009. The crystal structure of the ribosome bound to EF-Tu and aminoacyl-tRNA. *Science* **326:** 688–694.

Schneider-Poetsch T, Ju J, Eyler DE, Dang Y, Bhat S, Merrick WC, Green R, Shen B, Liu JO. 2010. Inhibition of eukaryotic translation elongation by cycloheximide and lactimidomycin. *Nat Chem Biol* **6:** 209–217.

SirDeshpande BV, Toogood PL. 1995. Mechanism of protein synthesis inhibition by didemnin B in vitro. *Biochemistry* **34:** 9177–9184.

Stanley WM Jr. 1974. Specific aminoacylation of the methionine-specific tRNA's of eukaryotes. *Methods Enzymol* **29:** 530–547.

Taraboletti G, Poli M, Dossi R, Manenti L, Borsotti P, Faircloth GT, Broggini M, D'Incalci M, Ribatti D, Giavazzi R. 2004. Antiangiogenic activity of aplidine, a new agent of marine origin. *Br J Cancer* **90:** 2418–2424.

Thornton S, Anand N, Purcell D, Lee J. 2003. Not just for housekeeping: Protein initiation and elongation factors in cell growth and tumorigenesis. *J Mol Med* **81:** 536–548.

Urdiales JL, Morata P, Nunez De Castro I, Sanchez-Jimenez F. 1996. Antiproliferative effect of dehydrodidemnin B (DDB), a depsipeptide isolated from Mediterranean tunicates. *Cancer Lett* **102:** 31–37.

Watabe M, Kakeya H, Onose R, Osada H. 2000. Activation of MST/Krs and c-Jun N-terminal kinases by different signaling pathways during cytotrienin A-induced apoptosis. *J Biol Chem* **275:** 8766–8771.

Wendel HG, De Stanchina E, Fridman JS, Malina A, Ray S, Kogan S, Cordon-Cardo C, Pelletier J, Lowe SW. 2004. Survival signalling by Akt and eIF4E in oncogenesis and cancer therapy. *Nature* **428:** 332–337.

Wolf H, Chinali G, Parmeggiani A. 1977. Mechanism of the inhibition of protein synthesis by kirromycin. Role of elongation factor Tu and ribosomes. *Eur J Biochem* **75:** 67–75.

Wurmbach P, Nierhaus KH. 1979. Codon-anticodon interaction at the ribosomal P (peptidyl-tRNA) site. *Proc Natl Acad Sci* **76:** 2143–2147.